KUNS 1320
January 1995

Structure of Li and Be isotopes studied with antisymmetrized molecular dynamics

Yoshiko Kanada-En'yo, Hisashi Horiuchi, and Akira Ono

Department of Physics, Kyoto University, Kyoto 606-01, Japan

Structure of odd-even and even-even isotopes of Li and Be is studied systematically with antisymmetrized molecular dynamics which is a theoretical method free from any model assumptions such as the existence of clustering. The construction of energy-minimum intrinsic states with definite parity is made by the use of the frictional cooling method. Angular momentum projection is applied to these intrinsic states in order to get eigenstates of angular momentum. It is shown that the clustering structure appears in the $N \approx Z$ region with N and Z standing for the neutron and proton numbers, respectively. But as N increases the structure is found to change toward the shell-model-like structure around $N \approx 8$. Furthermore possible existence of new-type clustering feature is suggested in further neutron-richer region with $N > 8$. Energy spectra and other quantities are shown to be reproduced well. Especially magnetic moments are shown to be very well reproduced and it is explained that the neutron number dependence of the observed magnetic moments reflects well the structure-change of the isotopes from the clustering structure to the shell-model-like structure. Important roles of the density dependence of the effective interaction are indicated.

PACS number(s): 21.10.-k, 27.20.+n

I. INTRODUCTION

A lot of information about neutron-rich nuclei has been obtained by recent experiments with radioactive nuclear beams [1-4]. It is desirable that those newly observed properties of neutron-rich nuclei are systematically studied in a single theoretical framework which can also describe ordinary nuclei, because we expect that such systematic study can give us the direct check whether theoretical understanding of unfamiliar features of exotic nuclei is consistent or not with that of ordinary nuclei. However little systematic theoretical research has been carried out for light nuclei.

Most theoretical studies about neutron-rich nuclei have concentrated on one nucleus or a few nuclei at most. For example some three-body model approaches [5] have been applied to ^{11}Li regarding it as ^{9}Li+$2n$ system and also applied to ^{6}He regarding it as α+$2n$ system. However, these models are not necessarily useful for other Li and He isotopes. Furthermore, in the case of ^{11}Li, there is left an important problem of treating ^{9}Li core excitation, although these models have succeeded in giving a realistic description of the neutron-halo structure [6-8] of this nucleus. Variational shell model [9] has been successfully used to study the system of ^{11}Be which is also considered to have the neutron-halo structure. It is not clear, however, whether this model is useful or not for the other Be isotopes with a remarkable cluster structure such as ^{8}Be.

There are many other neutron-rich nuclei which have been left hardly studied yet. The binding energies of neutrons of these nuclei show that some of them may have the neutron-halo structure. It is very well known that, in the $N \approx Z$ region with N and Z standing for the neutron and proton numbers, respectively, the clustering structure appears as is seen in the $t + \alpha$ cluster structure of ^{7}Li and in the $\alpha + \alpha$ cluster structure of ^{8}Be [10-14]. However little has been theoretically investigated about the existence of the cluster structure in the neutron-rich side of Li and Be isotopes. The recent experimental developments demand the theoretical research about these unsolved problems in the neutron-rich exotic region.

For most theoretical frameworks in light nuclei, it is not easy to make systematic researches on isotopes ranging from ordinary nuclei to neutron-rich nuclei. First of all, the applicability of mean field approach is not necessarily assured in light nuclei due to the existence of cluster structure. In fact it is very difficult for the shell model to describe such light nuclei as ^{7}Li and ^{8}Be which are known to have well-developed cluster structure. These ordinary light nuclei with cluster structure have been well studied with the cluster model. In the cluster model the existence of clusters is assumed from the beginning, that makes

the cluster model difficult to be used for the study of exotic nuclei for which we have little information or data. If a nucleus has shell-model-like structure instead of cluster structure, the cluster model does not provide a good approach. To make a systematic research on isotopes ranging from ordinary nuclei to neutron-rich exotic nuclei, it is desirable to use a theoretical framework which can describe both shell-model-like states and cluster-like states. The method of Antisymmetrized Molecular Dynamics (AMD) [15-21] is the very theoretical framework that satisfies these requirements and enables us to study isotopes of light nuclei systematically in *one framework* without any model assumptions.

AMD is a theory which has been developed recently intending originally to construct a new microscopic simulation method for the study of heavy ion reactions. Contrary to other microscopic simulation methods for heavy ion reactions [28,29], AMD is a quantum mechanical method since it describes the time development of the system wave function. The total wave function of AMD is a Slater determinant of single particle wave functions represented by Gaussian wave packets. AMD describes the reaction process by calculating the time evolution of the $6A$ variables representing the position and momentum centers of the Gaussian wave packets. The initialization of the collision calculation, namely the construction of the ground state wave functions of colliding nuclei, demands us to determine these variables for the the ground state wave functions. It is made by the frictional cooling method which is a kind of variational calculation. The method to construct the minimum energy wave function by the use of the frictional cooling technique in AMD provides us with a novel and powerful tool for the nuclear structure study because we have no need at all to rely on model assumptions. According to some preliminary studies [15,16], the AMD wave functions obtained by the frictional cooling method can describe well both the shell-model-like structure and the clustering structure. For instance, the AMD wave function of the ^{16}O ground state has proved to be of the double closed shell configuration, $(0s)^4(0p)^{12}$, and that of the ^{8}Be ground state has proved to have a well-developed dumbbell structure of $\alpha + \alpha$. Recently AMD was successfully applied to the study of the structure change along the yrast line of ^{20}Ne [27]. In this study the cranked intrinsic state was constructed for each spin-parity state along the yrast line by the use of the frictional cooling method with constraint on the expectation value of the angular momentum. This AMD approach enabled us, for the first time without introducing any model assumption, to describe the quite dramatic change of structure along the ^{20}Ne yrast line: namely the α+^{16}O clustering structure in low-spin region, the $(sd)^4$ shell-model-like structure around the band terminal 8^+ state, and

the appearance of "^{12}C + 2α"-like structure in 10^+ and 12^+ states.

The purpose of this paper is to study systematically the structure of Li and Be isotopes with AMD which is free from any model assumptions. By virtue of the use of AMD, we expect that we can trace the structure-change along the increase of the neutron number N even if the structure-change is so drastic as the change from the cluster structure to the shell-model-like structure. Specific problems we expect to elucidate in our systematic study of these isotopes include the following ones: We expect we can answer the question whether the clustering structure observed in the $N \approx Z$ region persists or fades out as N increases. Another question to be answered is why the magnetic moment of the exotic nucleus ^{11}Li with neutron halo is close to the Schmidt value while that of the ordinary nucleus ^{7}Li is fairly different from the Schmidt value.

As for the problem about the formation and dissolution of clusters in neutron-rich nuclei, we have a pioneering work by Seya, Kohno, and Nagata [30] on Be and B isotopes. In this work of Ref.[30], the molecular orbital model was adopted which described the system as composed of an α-α core and surrounding neutrons (and proton in B isotopes). It was found that the distance between two α's changed, along the increase of N, from the large values in ^{8}Be and ^{9}B to the very small values in ^{12}Be and ^{13}B which have the magic number $N = 8$ for neutrons. Furthermore, as a very interesting result, it was found that the α-α distance increased again as N increased beyond $N = 8$ toward the neutron dripline. A drawback of this pioneering work is that the existence of an α-α core was postulated from the beginning. In our present approach with AMD, we can check whether this postulation is justified or not. Especially, we expect that we can answer how plausible the existence of the clustering feature is in the neutron dripline region.

This paper is organized as follows. In the next section (Sec.II) we explain the formulation of AMD for our present study of nuclear structure. Namely we explain the AMD wave function, the frictional cooling method, and the angular momentum projection. In AMD for the structure study, we use not only a single Slater determinant for the wave function but also a superposition of Slater determinants. In some cases, it is important to make the superposition after the angular momentum projection. In Sec.III, the two-nucleon interaction used in this paper is explained. The calculated results are given and are compared with data in Sec.IV. Energy spectra and other quantities are shown to be well reproduced. Especially the systematical change of the observed magnetic dipole moments are excellently reproduced. It will be shown that the density dependent interaction is often important to

explain the observed data. We will show that the superposition of AMD Slater determinants describes the long tail of the wave function in two cases, the neutron halo structure in ^{11}Be and the outer tail of the relative wave function of α-t clusters in ^{7}Li. In Sec.V we will discuss the systematical change of the intrinsic states. The calculation results show the well-developed cluster structure in the nuclei with $N \sim Z$ and the shell-model-like structure in the nuclei with the neutron magic number $N = 8$. It means that the shell effects of neutron orbits play an important role in the structure of neutron-rich nuclei. The change of the observed magnetic moment from ^{7}Li to ^{11}Li is explained mainly by the change of the clustering structure of ^{7}Li to the shell-model-like structure of ^{11}Li. Possible existence of clustering feature is seen in the neutron-richer nuclei like ^{14}Be. Finally in Sec.VI we give summarizing discussions.

II. FORMULATION OF AMD

The AMD (Antisymmetrized Molecular Dynamics) is a theory which is applicable both to nuclear structure problems and to heavy-ion collision problems. Here we only explain the AMD framework for the sake of nuclear structure study. As for the AMD theory for the sake of nuclear reaction study, the reader is referred to Refs. [18] and [19]. Since the AMD framework for the structure study has recently been given also in Ref.[27], our explanation here is brief within keeping a self-contained style.

A. Wave function of AMD

In AMD the wave function of A-nucleon system $|\Phi\rangle$ is expressed by a Slater determinant,

$$|\Phi(\mathbf{Z})\rangle = \frac{1}{\sqrt{A!}}\det\Big[\varphi_j(i)\Big], \quad \varphi_j = \phi_{\mathbf{Z}_j}\chi_{\alpha_j}, \tag{1}$$

where χ_{α_j} is the spin isospin wave function of j-th single particle state, where α_j indicates the spin isospin, $\alpha_j = \mathrm{p}\uparrow, \mathrm{p}\downarrow, \mathrm{n}\uparrow,$ or $\mathrm{n}\downarrow$. The spatial wave function of the j-th single particle state $\phi_{\mathbf{Z}_j}$ is represented by a Gaussian wave packet,

$$\begin{aligned}\langle \mathbf{r}|\phi_{\mathbf{Z}_j}\rangle &= \left(\frac{2\nu}{\pi}\right)^{3/4}\exp\left[-\nu\left(\mathbf{r} - \frac{\mathbf{Z}_j}{\sqrt{\nu}}\right)^2 + \frac{1}{2}\mathbf{Z}_j^2\right], \\ &\propto \exp[-\nu(\mathbf{r} - \mathbf{D}_j)^2 + \frac{i}{\hbar}\mathbf{K}_j\cdot\mathbf{r}], \\ \mathbf{Z}_j &= \sqrt{\nu}\mathbf{D}_j + \frac{i}{2\hbar\sqrt{\nu}}\mathbf{K}_j,\end{aligned} \tag{2}$$

whose center is expressed with a complex parameter $\mathbf{Z}_j$, where ν is the width of the wave

packet common to all nucleons. Thus the wave function of the system $|\Phi(\mathbf{Z})\rangle$ is parameterized by complex parameters $\{\mathbf{Z}\} = \{\mathbf{Z}_1, \mathbf{Z}_2, \ldots, \mathbf{Z}_A\}$.

The wave function $|\Phi(\mathbf{Z})\rangle$ of Eq.(1) is the same as the wave function of the Fermionic Molecular Dynamics proposed by Feldmeier [31]. Furthermore, $|\Phi(\mathbf{Z})\rangle$ can be regarded as a special case of the Brink-type cluster model wave function [32] where every cluster is composed of a single nucleon. When the parameters of the Brink-type wave function are treated as time-dependent parameters by using the time-dependent variational principle, the Brink-type cluster model is called the time-dependent cluster model (TDCM) [33]. Therefore, $|\Phi(\mathbf{Z})\rangle$ can be also regarded as a special case of the TDCM wave function. The reason we use the name AMD for our present approach to nuclear structure problems is mainly because our approach is characteristic in the point that it is always combined with the frictional cooling method which determines the parameters of the wave function often under given constraints. Other characteristic points of our approach are the use of projection of parity and angular momentum and the frequent use of the superposition of Slater determinants. (In the case of heavy-ion collision problems, the reason why we use the name AMD is mainly because our approach is characteristic in the point that the stochastic two-nucleon collisions are treated by introducing the physical nucleon coordinates.)

For the study of nuclear structure, the AMD wave function $|\Phi(\mathbf{Z})\rangle$ explained above is projected to the parity eigenstate,

$$|\Phi^{\pm}(\mathbf{Z}_1, \mathbf{Z}_2, \ldots, \mathbf{Z}_A)\rangle = (1 \pm P)|\Phi(\mathbf{Z}_1, \mathbf{Z}_2, \ldots, \mathbf{Z}_A)\rangle, \tag{3}$$

with P standing for the parity inversion operator. Since different parity states of a nucleus usually have different structures, this projection is indispensable to discuss the structure of each parity state. Furthermore we often make a linear combination of two AMD Slater determinants for more precise study of the nuclear structure,

$$|\Phi^{\pm}(\mathbf{Z}_1, \ldots, \mathbf{Z}_A, \mathbf{Z}'_1, \ldots, \mathbf{Z}'_A, C)\rangle = |\Phi^{\pm}(\mathbf{Z}_1, \ldots, \mathbf{Z}_A)\rangle + C|\Phi^{\pm}(\mathbf{Z}'_1, \ldots, \mathbf{Z}'_A)\rangle. \tag{4}$$

Note that the number of complex parameters of the wave function of Eq.(4) is $6A + 1$ while that of the original AMD is $3A$. In this paper, for the sake of convenience, we call the wave function of Eq.(3) simply as AMD wave function, and the latter one in Eq.(4) as Extended AMD (EAMD) wave function.

B. Frictional cooling method

As mentioned in subsection A, the AMD wave function of a system $|\Phi^{\pm}(\mathbf{Z})\rangle$ is parameterized by the centers of Gaussian wave packets $\{\mathbf{Z}\} = \{\mathbf{Z}_1, \mathbf{Z}_2, \ldots, \mathbf{Z}_A\}$. Let us consider to construct the ground state wave function of the system. First we choose some initial parameters $\{\mathbf{Z}\}$ of all A nucleons rather arbitrarily. The initial wave function $|\Phi^{\pm}(\mathbf{Z})\rangle$ with this initial choice of $\{\mathbf{Z}\}$ represents in general a highly excited state. We should determine the parameters $\{\mathbf{Z}\}$ which give the minimum energy for the expectation value of the Hamiltonian H

$$\widehat{E} = \widehat{E}(\mathbf{Z}, \mathbf{Z}^*) \equiv \frac{\langle\Phi^{\pm}(\mathbf{Z})|H|\Phi^{\pm}(\mathbf{Z})\rangle}{\langle\Phi^{\pm}(\mathbf{Z})|\Phi^{\pm}(\mathbf{Z})\rangle}. \tag{5}$$

For this purpose we introduce frictional cooling equations for $\{\mathbf{Z}\}$ expressed as

$$\frac{d\mathbf{Z}_k}{dt} = (\lambda + i\mu)\frac{1}{i\hbar}\frac{\partial\widehat{E}}{\partial\mathbf{Z}_k^*} \qquad \text{and} \qquad c.c. \ , \tag{6}$$

with arbitrary real numbers λ and $\mu < 0$. It is easily proved that the energy decreases with time if the system follows this equation;

$$\begin{aligned}\frac{d\widehat{E}}{dt} &= \sum_{i=1}^{A}\frac{\partial\widehat{E}}{\partial\mathbf{Z}_i}\cdot\frac{d\mathbf{Z}_i}{dt} + \frac{\partial\widehat{E}}{\partial\mathbf{Z}_i^*}\cdot\frac{d\mathbf{Z}_i^*}{dt} \\ &= \frac{2\mu}{\hbar}\sum_{i=1}^{A}\frac{\partial\widehat{E}}{\partial\mathbf{Z}_i}\cdot\frac{\partial\widehat{E}}{\partial\mathbf{Z}_i^*} < 0.\end{aligned} \tag{7}$$

Then the wave function of the minimum energy state is obtained after sufficient cooling time. This cooling method explained above is called the frictional cooling method. Obviously the frictional cooling method can be used not only in the AMD but also in the general variational calculation with any kind of wave functions which are parameterized by complex parameters. Therefore just in the same way as AMD, we can obtain the minimum energy state of the Extended AMD wave function described in subsection A.

C. Constrained frictional cooling method

The frictional cooling method can be extended so as to construct the minimum energy state with a given constraint. The constraint is written by a constraint function as

$$\widehat{W} = \widehat{W}(\mathbf{Z}^*, \mathbf{Z}) = \text{given number.} \tag{8}$$

The constraint function is restricted to be real. An example of the constraint is the magnitude

of the orbital angular momentum. In this case the constraint function $\widehat{W}(\mathbf{Z}^*, \mathbf{Z})$ is chosen to be

$$\begin{aligned}\widehat{W}(\mathbf{Z}^*, \mathbf{Z}) &= \widehat{\mathbf{L}}(\mathbf{Z}^*, \mathbf{Z})\cdot\widehat{\mathbf{L}}(\mathbf{Z}^*, \mathbf{Z}), \\ \widehat{\mathbf{L}}(\mathbf{Z}^*, \mathbf{Z}) &= \frac{\langle\Phi^{\pm}(\mathbf{Z})|\sum_{j=1}^{A}\left(\mathbf{r}_j\times(-i)\frac{\partial}{\partial\mathbf{r}_j}\right)|\Phi^{\pm}(\mathbf{Z})\rangle}{\langle\Phi^{\pm}(\mathbf{Z})|\Phi^{\pm}(\mathbf{Z})\rangle}.\end{aligned} \tag{9}$$

First we assume that we have initial coordinates $\{\mathbf{Z}^{\text{int}}\}$ which satisfy the given condition;

$$\widehat{W}(\mathbf{Z}^{\text{int}*}, \mathbf{Z}^{\text{int}}) = \text{given number.}$$

We introduce the following frictional cooling equation instead of Eq.(6);

$$\frac{d\mathbf{Z}_k}{dt} = (\lambda + i\mu)\frac{1}{i\hbar}\left(\frac{\partial\widehat{E}}{\partial\mathbf{Z}_k^*} + \eta\frac{\partial\widehat{W}}{\partial\mathbf{Z}_k^*}\right) \qquad \text{and} \qquad c.c. \ , \tag{10}$$

with arbitrary real numbers λ and $\mu < 0$. The multiplier function η is determined by the condition of conserving the value of the constraint function $\widehat{W}$;

$$\frac{d}{dt}\widehat{W}(\mathbf{Z}^*, \mathbf{Z}) = 0. \tag{11}$$

By using Eq.(10) we have

$$\begin{aligned}\frac{d}{dt}\widehat{W}(\mathbf{Z}^*, \mathbf{Z}) &= \sum_{j=1}^{A}\left(\frac{\partial\widehat{W}}{\partial\mathbf{Z}_j}\frac{d\mathbf{Z}_j}{dt} + \frac{\partial\widehat{W}}{\partial\mathbf{Z}_j^*}\frac{d\mathbf{Z}_j^*}{dt}\right) \\ &= (\lambda + i\mu)\frac{1}{i\hbar}\sum_{j=1}^{A}\left(\frac{\partial\widehat{W}}{\partial\mathbf{Z}_j}\cdot\frac{\partial\widehat{E}}{\partial\mathbf{Z}_j^*} + \eta\frac{\partial\widehat{W}}{\partial\mathbf{Z}_j}\cdot\frac{\partial\widehat{W}}{\partial\mathbf{Z}_j^*}\right) \\ &+ (\lambda - i\mu)\frac{-1}{i\hbar}\sum_{j=1}^{A}\left(\frac{\partial\widehat{W}}{\partial\mathbf{Z}_j^*}\cdot\frac{\partial\widehat{E}}{\partial\mathbf{Z}_j} + \eta\frac{\partial\widehat{W}}{\partial\mathbf{Z}_j^*}\cdot\frac{\partial\widehat{W}}{\partial\mathbf{Z}_j}\right)\end{aligned} \tag{12}$$

Hence from Eqs.(11) and (12) η is determined as follows

$$\begin{aligned}\eta &= -\frac{\mathcal{G}}{\mathcal{F}}, \quad \mathcal{F} = 2\sum_{j=1}^{A}\frac{\partial\widehat{W}}{\partial\mathbf{Z}_j}\cdot\frac{\partial\widehat{W}}{\partial\mathbf{Z}_j^*}, \\ \mathcal{G} &= \sum_{j=1}^{A}\left[(1 - i\frac{\lambda}{\mu})\frac{\partial\widehat{W}}{\partial\mathbf{Z}_j}\cdot\frac{\partial\widehat{E}}{\partial\mathbf{Z}_j^*} + (1 + i\frac{\lambda}{\mu})\frac{\partial\widehat{W}}{\partial\mathbf{Z}_j^*}\cdot\frac{\partial\widehat{E}}{\partial\mathbf{Z}_j}\right].\end{aligned} \tag{13}$$

Cooling of the total energy is assured for arbitrary λ if μ is negative, because there holds

the following relation

$$\begin{aligned}\frac{d}{dt}\widehat{E} &= \sum_k \left(\frac{\partial \widehat{E}}{\partial \mathbf{Z}_k^*}\frac{d\mathbf{Z}_k^*}{dt} + \frac{\partial \widehat{E}}{\partial \mathbf{Z}_k}\frac{d\mathbf{Z}_k}{dt} \right) \\ &= \sum_k \left[\left(\frac{\hbar}{\mu - i\lambda}\frac{d\mathbf{Z}_k}{dt} - \eta \frac{\partial \widehat{W}}{\partial \mathbf{Z}_k^*} \right)\frac{d\mathbf{Z}_k^*}{dt} + \left(\frac{\hbar}{\mu + i\lambda}\frac{d\mathbf{Z}_k^*}{dt} - \eta \frac{\partial \widehat{W}}{\partial \mathbf{Z}_k} \right)\frac{d\mathbf{Z}_k}{dt} \right] \\ &= \frac{2\mu\hbar}{\mu^2+\lambda^2}\sum_k \frac{d\mathbf{Z}_k^*}{dt}\frac{d\mathbf{Z}_k}{dt} - \eta\frac{d}{dt}\widehat{W} \\ &= \frac{2\mu\hbar}{\mu^2+\lambda^2}\sum_k \frac{d\mathbf{Z}_k^*}{dt}\frac{d\mathbf{Z}_k}{dt} < 0,\end{aligned} \tag{14}$$

with arbitrary real numbers λ and $\mu < 0$.

It is easy to extend this constrained frictional cooling method to the general case with many constraints and also to the Extended AMD wave function.

The most important feature of the construction of the wave function in AMD by the use of the frictional cooling method with or without the constraint is that the wave function can be obtained without prejudice, i.e., free from any model assumptions such as the existence of clustering. If the resulting wave function proves to have clustering structure, the existence of clustering can be insisted more convincingly than other usual cluster model studies. AMD is a new powerful method for the study of the formation and dissolution of clusters in nuclei.

D. Use of constrained frictional cooling method in the actual calculation of Extended AMD

When we make calculations of the frictional cooling in the framework of the Extended AMD (EAMD), we usually encounter the following problem. Let us consider our present EAMD calculation in which we adopt a superposition of two AMD Slater determinants $|\Phi_1^{\pm}(\mathbf{Z})\rangle$ and $|\Phi_2^{\pm}(\mathbf{Z}')\rangle$. In many cases, $|\Phi_1^{\pm}(\mathbf{Z})\rangle$ and $|\Phi_2^{\pm}(\mathbf{Z}')\rangle$ after the frictional cooling have proved to be the same except the difference of their spatial orientations. However, as we explain in the next subsection, in our AMD study we always make angular momentum projection from the AMD and EAMD wave functions in order to get eigenstates of the total angular momentum. Therefore the above EAMD result that $|\Phi_1^{\pm}(\mathbf{Z})\rangle$ and $|\Phi_2^{\pm}(\mathbf{Z}')\rangle$ are the same except their spatial orientations does not meet the aim of the EAMD calculation to improve the AMD calculation.

The method which we adopt in this paper to avoid the above-mentioned difficulty of the EAMD is to impose a constraint to the frictional cooling procedure. The constraint

is that the spatial orientations of $|\Phi_1^{\pm}(\mathbf{Z})\rangle$ and $|\Phi_2^{\pm}(\mathbf{Z}')\rangle$ should be the same. The spatial orientations of $|\Phi_1^{\pm}(\mathbf{Z})\rangle$ and $|\Phi_2^{\pm}(\mathbf{Z}')\rangle$ are defined in the following way. As we will report later in this paper, the AMD results show that in Li isotopes wave-packet centers of two protons with spin up and down are located at almost the same spatial points and the last proton wave-packet center is located at a different spatial point, while in Be isotopes we have spatially separated two pairs of protons with spin up and down and within each pair two protons are located closely to each other. Therefore as the definition of the orientation of the AMD wave function for Li and Be isotopes, we adopt the direction which connects two groups of protons.

The constraint function $\widehat{W}(\mathbf{Z}^*, \mathbf{Z}'^*, \mathbf{Z}, \mathbf{Z}')$ is given as follows,

$$\begin{aligned}&\widehat{W}(\mathbf{Z}^*, \mathbf{Z}'^*, \mathbf{Z}, \mathbf{Z}') = \frac{\mathbf{Y}\cdot\mathbf{Y}'}{\|\mathbf{Y}\|\cdot\|\mathbf{Y}'\|}, \\ &\mathbf{Y} \equiv \frac{1}{n(G_1)}\sum_{j\in G_1}\mathrm{Re}\mathbf{Z}_j - \frac{1}{n(G_2)}\sum_{j\in G_2}\mathrm{Re}\mathbf{Z}_j, \\ &\mathbf{Y}' \equiv \frac{1}{n(G_1)}\sum_{j\in G_1}\mathrm{Re}\mathbf{Z}'_j - \frac{1}{n(G_2)}\sum_{j\in G_2}\mathrm{Re}\mathbf{Z}'_j,\end{aligned} \tag{15}$$

where G_1 and G_2 stand for two groups of protons explained above, and $n(G_1)$ and $n(G_2)$ are numbers (one or two) of protons contained in the groups G_1 and G_2, respectively. Here, of course, wave packet centers $\{\mathbf{Z}_j\}$ and $\{\mathbf{Z}'_j\}$ are those of $|\Phi_1^{\pm}(\mathbf{Z})\rangle$ and $|\Phi_2^{\pm}(\mathbf{Z}')\rangle$, respectively. Initial coordinates $\{\mathbf{Z}_j^{\mathrm{int}}\}$ and $\{\mathbf{Z}_j'^{\mathrm{int}}\}$ for the procedure of the constrained frictional cooling are chosen so as to satisfy $\widehat{W}(\mathbf{Z}^{\mathrm{int}*}, \mathbf{Z}'^{\mathrm{int}*}, \mathbf{Z}^{\mathrm{int}}, \mathbf{Z}'^{\mathrm{int}}) = 1$, but the protons belonging to the same group G_1 or G_2 need not to be located closely to each other in the initial configurations $\{\mathbf{Z}_j^{\mathrm{int}}\}$ and $\{\mathbf{Z}_j'^{\mathrm{int}}\}$.

E. Projection to total angular momentum eigenstates

The wave function of the system should be a total-angular-momentum eigenstate. It is however difficult to cool the total-angular-momentum projected state of AMD wave function. We regard the minimum energy state which is obtained with the cooling method described in subsections B and C as the intrinsic state of the system. We project the intrinsic wave function $|\Phi^{\pm}\rangle$ to the total-angular-momentum eigenstates, and then calculate the expectation

values of operators in order to compare with experimental data;

$$\frac{\langle P^J_{MK}\Phi^{\pm}|\hat{T}^k_{q=0}|P^J_{MK}\Phi^{\pm}\rangle}{\langle P^J_{MK}\Phi^{\pm}|P^J_{MK}\Phi^{\pm}\rangle} = \frac{\mathcal{T}}{\mathcal{N}},$$
$$\mathcal{T} = (JMk0|JM)\sum_{K'\nu}(JK'k\nu|JK)\int d\Omega D^{J*}_{K'K}(\Omega)\langle\Phi^{\pm}|\hat{T}^k_{\nu}R(\Omega)|\Phi^{\pm}\rangle, \qquad (16)$$
$$\mathcal{N} = \int d\Omega D^{J*}_{KK}(\Omega)\langle\Phi^{\pm}|R(\Omega)|\Phi^{\pm}\rangle,$$

where P^J_{MK} is a total-angular-momentum projection operator,

$$P^J_{MK} \equiv \int d\Omega D^{J*}_{MK}(\Omega)R(\Omega), \qquad (17)$$

with $R(\Omega)$ standing for the rotation operator by Euler angle Ω, and $\hat{T}^k_q$ is a given tensor operator of rank k. K should be chosen so as to get the minimum expectation value of the Hamiltonian in each system. The K-mixing, namely the diagonalization of the Hamiltonian with respect to the K quantum number is not made in most cases, but in some cases we show results obtained by K-mixing calculation. The spin J of the calculated ground state has been found to be the same as the observed spin value of the ground state for almost every system studied here. In the practical calculation, the three-dimensional integral is evaluated numerically by taking finite number of mesh points of the Euler angle Ω.

III. INTERACTION

For the effective two-nucleon interaction, we have adopted Volkov No.1 force [34] as the central force. The Volkov force contains only Wigner and Majorana components. For some nuclei treated in this paper, we have made calculations by adding appropriate Bartlett and Heisenberg components to the Volkov force. But the results have proved to be not so much affected by the additional components at least for the quantities studied in this paper. We are now making more detailed investigations about this point which will be reported elsewhere. As for the two-body spin-orbit force V_{LS} we have adopted the G3RS force [35] expressed as

$$V_{LS} = \{u_I\exp(-\kappa_I\mathbf{r}^2) + u_{II}\exp(-\kappa_{II}\mathbf{r}^2)\}P(^3O)\mathbf{L}\cdot(\mathbf{S}_1+\mathbf{S}_2),$$
$$\mathbf{L} \equiv \mathbf{r}\times(-i\frac{\partial}{\partial\mathbf{r}}), \quad u_I = -u_{II} = 900 \text{ MeV}, \qquad (18)$$
$$\kappa_I = 5.0 \text{ fm}^{-2}, \quad \kappa_{II} = 2.778 \text{ fm}^{-2},$$

with $\mathbf{r}$ denoting the two-nucleon relative coordinate and with $P(^3O)$ denoting the projection

operator onto the triplet odd (^3O) two-nucleon state. Coulomb interaction is approximated by a sum of seven Gaussians following the technique of Ref.[19]. This approximation is valid for the range of the inter-nucleon distance from 1 fm to 20 fm, and is precise enough for the study of nuclear structure. In order to study the effect of the density dependent interaction, we have also used the case 3 of the MV1 force of Ref.[36] which contains a zero-range three-body interaction $V^{(3)}_{DD}$ in addition to the two-body interaction $V^{(2)}_{DD}$:

$$V^{(2)}_{DD} = (1 - m - mP_\sigma P_\tau)\left[V_A\exp(-(\frac{r}{r_A})^2) + V_R\exp(-(\frac{r}{r_R})^2)\right],$$
$$V_A = -83.34 \text{ MeV}, \quad r_A = 1.60 \text{ fm}, \quad V_R = 104.86 \text{ MeV}, \quad r_R = 0.82 \text{ fm}, \qquad (19)$$
$$V^{(3)}_{DD} = v^{(3)}\delta(\mathbf{r}_1-\mathbf{r}_2)\delta(\mathbf{r}_1-\mathbf{r}_3), \quad v^{(3)} = 4000 \text{ MeV}\cdot\text{fm}^6,$$

where P_σ and P_τ stand for the spin and isospin exchange operators, respectively. The two-body interaction part $V^{(2)}_{DD}$ is constructed from the Volkov No.1 force by weakening the strength of its repulsive part from $V_R = 144.86$ MeV to $V_R = 104.86$ MeV. We have compared the results with and without the three body interaction. The optimum width parameter ν of wave packets is chosen for each parity of the individual system so as to get the minimum energy.

IV. CALCULATED RESULTS AND COMPARISON WITH EXPERIMENTS

The structure of odd-even and even-even isotopes of Li and Be have been studied with AMD and the results are reported in this section. For Be isotopes, studies have been made also with the Extended AMD. We have checked the values of the momentum parameters $\{\mathbf{K}_j,\ j=1,\ldots,A\}$ of the AMD wave function obtained with the frictional cooling method and have found that $\{\mathbf{K}_j\}$ parameters of all the nucleons are small in all the nuclei studied here .

A Binding energies and energy spectra

Figure 1 shows the binding energies of the ground states of Li and Be isotopes. We have used the Majorana parameter $m = 0.56$ in the case of no three-body force (Volkov force) and $m = 0.576$ with the three-body force (MV1 force). The optimum width parameters ν are shown in Table I. With both the interactions, binding energies are qualitatively reproduced for Li isotopes and also for Be isotopes except for ^{11}Be. In Li isotopes the MV1

force gives better fitting to data. The calculated result of ^{11}Be is that of the lowest $\frac{1}{2}^+$ state. Detailed discussions about the energy and the parity of the ^{11}Be ground state will be given later. For the discussion of the neutron halo structure, it is important to precisely reproduce relative binding energies between neighboring nuclei, since the density tail of the neutron halo must be very sensitive to the binding energy of valence neutrons. Hence for the study of neutron halo structure, it is necessary to give careful consideration in choosing the interaction parameters because the energies depend rather sensitively on some parameters such as Majorana parameter for the Volkov force.

The calculated energy spectra with and without the three-body interaction are shown and are compared with the observed data in Fig.2 for Li isotopes and in Fig.3 for Be isotopes. The second $J^\pm$ levels with the three-body force are obtained by diagonalizing the Hamiltonian matrix with respect to the K quantum number in the spin J projected states. For the lowest $J^\pm$ states the diagonalization of the Hamiltonian gives almost the same energy spectra as the spectra without the K-mixing. This means that K is approximately a good quantum number in the lowest $J^\pm$ states projected from the AMD wave functions. The spectra with the three-body force are found to have larger moment of inertia than those without the three-body force. The three-body force gives greater effects on the energy difference between normal parity and non-normal parity states and the calculation with the three-body interaction is seen to reproduce the energy spectra well except for ^{11}Be.

The results of the AMD calculation without the three-body force give larger value for this energy difference than the observed value in the system of most Li and Be isotopes. On the other hand, in the results with the three-body force the excitation energy of non-normal parity states come down and agree much better with the experimental data. In general non-normal parity states have wider extension of the density distribution and feel relatively weaker repulsive density-dependent force than normal-parity states. It is the reason why the calculation with the three-body force gives smaller excitation energy of non-normal parity states than that without the three-body force.

The density-dependent force seems to be important especially for the system of ^{11}Be. In terms of the shell model, the normal parity of the ^{11}Be system should be negative, but it is experimentally known that the ground state is a non-normal positive parity $\frac{1}{2}^+$ state and the lowest $\frac{1}{2}^-$ state is excited by 0.32 MeV. In the AMD results without the three-body force, the lowest $\frac{1}{2}^+$ state is not the ground state but is excited by about 7 MeV from the lowest $\frac{1}{2}^-$. With the three-body force, the lowest $\frac{1}{2}^+$ state has less excitation energy of about 5

MeV. Interaction parameters can be adjusted so as to get better agreement with data. For example when we use Majorana parameter $m = 0.65$, the calculated result becomes better and about 3 MeV is obtained as the excitation energy of the lowest $\frac{1}{2}^+$ state. The careful choice of the effective interaction is one of the important points for the reproduction of the non-normal parity ground state.

There are left other important problems. Fukunishi, Otsuka, and Sagawa [9] have studied the structure of ^{11}Be with the approach which they call the variational shell model and have obtained the positive parity ground state. They discussed that such a low excitation energy of the non-normal parity state largely owes to its deformation and to the neutron halo structure. Unfortunately it is not straightforward for the AMD to express the long tail of neutron halo structure because the single particle wave function of AMD is described with a simple Gaussian wave packet. A superposition of some AMD wave functions is necessary for this problem, and we have tried to make Extended AMD calculations with a superposition of two Slater determinants. The lowest positive parity state obtained with the EAMD, in which the neutron density distribution is spatially more extended, has about 0.5 MeV lower excitation energy than in the AMD calculation, but, the improvement of the excitation energy is too little to reproduce the positive parity ground state. Further extensions of the AMD wave function should be tried. By supposing that the AMD method can well describe the single particle wave functions of the nucleons other than the last valence neutron (or halo neutron) which is located at a somewhat isolated position from other nucleons, we have adopted the following method in order to see what structure is prefered by the last valence neutron in the lowest positive parity state of ^{11}Be. The single particle wave functions of the other ten nucleons have been fixed to be the same as the AMD result of ^{11}Be. Only the wave function for the last valence neutron has been described by a superposition of some Gaussian wave packets which have the same width parameter ν but different centers $\mathbf{Z}_{11}$'s. We have determined the coefficient of each Gaussian in the superposition not by cooling but by diagonalyzing the matrix elements of the Hamiltonian. This method has been applied to each parity state of ^{11}Be. When the energies are compared before making the angular momentum projection, the excitation energy of the lowest positive parity state has become by 0.9 MeV smaller than in the AMD calculation. Since the neutron-halo structure is directly concerned with the radius of the nucleus, we will discuss the ^{11}Be problem again in the next subsection. In the neutron-richer nuclei of Be, some excited levels have been observed. But the spin parity J^π of many states have not been identified yet. The AMD calculation with

the density dependent force suggests that some states of non-normal parity may exist in the rather low excitation energy region in ^{12}Be which have deformed structure.

B. Radii of nuclei

Figure 4 shows the comparison of the theoretical values of the radii of Li and Be isotopes with experimental data. The calculated radius of ^{11}Be is that of the lowest $\frac{1}{2}^+$ state. Dotted lines are the AMD results without the three-body force, dashed lines the results with the three-body force, and solid lines the EAMD results with the three-body force.

Experimentally observed radii of Be-isotopes are seen to be qualitatively reproduced by the calculations of AMD with the three-body repulsive force, while without the three-body force the calculated radii are too small especially in neutron-rich systems. These results show that the density-dependent repulsive force is important to reproduce the large observed radii. We consider the reason is as follows: Since the three-body repulsive force works weaker in the low density region, the state prefers having the density distribution extended to spatially wider region, which results in the larger radius.

However even the AMD calculation with the three-body force can not sufficiently reproduce the large radii of neutron-rich nuclei such as ^{11}Be that extremely deviate from the $A^{1/3}$ law. Like the problem about the energy difference between different parity states in the ^{11}Be system discussed in the previous subsection, one of the important points for this problem of the large radius is the careful choice of the effective interaction that is to say the adjustment of interaction parameters. The nuclear radius as well as the binding energy is very sensitive to the choice of the effective interaction. For example, if we use the Majorana parameter $m = 0.65$ in the AMD calculation with the three-body force, the radius of the $\frac{1}{2}^+$ ^{11}Be state increases up to a large value, 2.78 fm, that is as large as the experimental value. In fact it is generally reasonable to adopt larger m value in a nucleus with larger mass number, and the use of the fixed value of the m parameter for all the isotopes is not necessarily justified. Hence the value $m = 0.65$ may not be so unnatural for ^{11}Be.

The extremely large radius of the ^{11}Be ground state is of course directly related to the neutron halo structure of this state. In the previous subsection, we have reported the calculation in which we have made the superposition of several Gaussians of the last valence neutron. This calculation has been made with the expectation that the reproduction of the long tail of the last valence neutron may reduce the large energy gap between different parity states. The radius obtained by this superposition calculation is 2.33 fm, which is only by

0.05 fm larger than the value obtained by the simple AMD calculation. On the other hand, much difference is found in the result of the neutron density distribution as shown in Fig.5. The dashed line shows the proton density distribution and the solid line shows the neutron one for the $\frac{1}{2}^+$ ^{11}Be state. Contrary to the proton density, the solid line of neutron density has a long tail with low density in the outer region from 5 fm to more than 10 fm. On the other hand, in the case of the simple AMD calculation, the neutron density distributes in almost the same way as the proton density and has no tail. However when compared with the phenomenologically-determined density distribution which provides a good fit to the cross section of the neutron dissociation reaction, the tail described in our result is by about one order smaller in the region around 10 fm. Here we should make a remark that the calculated $\frac{1}{2}^+$ ^{11}Be state still has a higher energy than the ^{10}Be+n threshold energy.

Also in the calculated results of Li-isotopes, the AMD and EAMD have not been able to sufficiently reproduce the large radius of ^{11}Li that deviates largely from the $A^{1/3}$ law. The small binding energy of ^{11}Li has been considered to be very important to describe its large radius. It implies the importance of the exact reproduction of the binding energy which is sensitive to the interaction parameters. Besides that, further extensions of the AMD wave function may be necessary for the precise description of the neutron-halo structure.

C. Magnetic moments

The calculated results of magnetic dipole moments are not sensitive to the interaction parameters except for ^{11}Be. Almost the same values are obtained with and without the three-body force in the AMD calculations and even in the EAMD calculations except for the ^{11}Be system. The results of the AMD calculation given in Fig.6 show very good agreement with the experimental values for even-odd isotopes of Li and Be. It should be emphasized that the AMD method is the first framework which has succeeded in reproducing the magnetic dipole moments systematically for these isotopes as long as we know.

The dependence on the neutron number seen in the observed values for Li isotopes is expected to carry important information on the nuclear structure, because in terms of the shell model the valence proton in the same $0p_{3/2}$ orbital would give dominant effects on the magnetic moments and hence almost the same value would be obtained for the magnetic moments of all these isotopes. We will give detailed discussions about the dependence on the neutron number of the system in the later section.

Contrary to Li isotopes, in the case of Be isotopes the wave function for the last valence

neutron may contribute mainly, and it is important to make a closer discussion of the neutron orbital itself. The magnetic dipole moment is measured only for ^{9}Be, and the result obtained with the AMD agrees well with the data. On the other hand, a little complicated problem exists in the system of ^{11}Be for which the experimental data have not been obtained yet. In the ^{11}Be system, two different states are eventually obtained with the AMD calculations. The two states have almost the same values of the binding energy and the root-mean-square radius, but they have considerably different magnetic dipole moments, -1.9 n.m. and -1.5 n.m.. In this situation, it is expected to be useful to apply the EAMD method with two Slater determinants of AMD wave functions. With the EAMD calculation, the result of -1.9 n.m. is obtained. However, the calculations by the use of different interaction parameters m and $u_I = -u_{II}$ of V_{LS} give various results ranging from -1.5 n.m. to -1.9 n.m.. We need more careful investigations in order to get a conclusion about the theoretical value for the magnetic moment of ^{11}Be, since there is left the problem to reproduce the observed large radius which is concerned with the neutron-halo structure.

D. Electric quadrupole moments and $B(E2)$ values

The electric quadrupole moments for even-odd isotopes of Li and Be calculated with the three-body force are shown in Fig.7 and are seen to reproduce well the experimental data. The AMD results without the three-body force are much smaller in absolute value than the experimental data. It is not surprising that this situation is similar to the case of the radii which have already been discussed in the subsection B. We can say that the small values of quadrupole moments obtained without the three-body force are mainly due to the problem not in the quadrupole deformation but in the radial density distribution. Although the values with the three-body force seem to be still slightly smaller than the data, it is not a serious problem, because about 10 percent larger values can be obtained just by using $m = 0.60$ as the Majorana parameter instead of $m = 0.576$.

The theoretical value of the quadrupole moment of ^{7}Li shown in Fig.7 has been obtained by improving the AMD wave function in the following way. As we discuss later in detail, the AMD wave function of ^{7}Li has proved to have a cluster structure of α+t. However, since the single nucleon wave function of AMD is a Gaussian wave packet, the relative wave function between α and t is also necessarily a Gaussian wave packet of the form,

$$\exp\left[-\frac{4\cdot 3}{4+3}\nu(\mathbf{X}_\alpha - \mathbf{X}_t - \mathbf{R})^2\right],$$
$$\mathbf{X}_\alpha \equiv \frac{1}{4}\sum_{j=1}^{4}\mathbf{r}_j, \quad \mathbf{X}_t \equiv \frac{1}{3}\sum_{j=5}^{7}\mathbf{r}_j, \tag{20}$$
$$\mathbf{R} = \frac{1}{4}\sum_{j=1}^{4}\mathbf{Z}_j - \frac{1}{3}\sum_{j=5}^{7}\mathbf{Z}_j.$$

When the clustering is well developed, the description of the inter-cluster relative wave function by a single Gaussian wave function is not sufficient because the relative wave function spreads out toward the outer spatial region resulting in a long tail. The lack of the outer tail part of the inter-cluster relative wave function may be sensitively reflected in the value of the quadrupole moment. In fact, the AMD with the three-body force has given us rather small value of the ^{7}Li quadrupole moment compared with the data. Therefore we have improved the inter-cluster relative wave function of the AMD wave function by superposing several AMD wave functions as described below. The trial AMD wave functions to be superposed have been constructed by adopting the following changes of the original $\{\mathbf{Z}\}$ values,

$$\mathbf{Z}_j \longrightarrow \mathbf{Z}_j + \frac{3}{7}\sqrt{\nu}\mathbf{C}, \quad \text{for } j = 1,\ldots,4,$$
$$\mathbf{Z}_j \longrightarrow \mathbf{Z}_j - \frac{4}{7}\sqrt{\nu}\mathbf{C}, \quad \text{for } j = 5,\ldots,7. \tag{21}$$

The trial AMD wave functions having different values of the displacement real vector $\mathbf{C}$ have been all projected onto the $\frac{3}{2}^-$ state in parity and angular momentum. The superposition of these projected states has been made by diagonalizing the total Hamiltonian. The resulting improved AMD wave function has proved to reproduce the quadrupole moment well as seen in Fig.7.

Table II shows the $E2$ transition strength compared with the observed data. The simple AMD calculations reproduce well the experimental data except for the strength $B(E2; 1/2^- \rightarrow 3/2^-)$ of ^{7}Li. The theoretical value 7.51 e^{2}fm^4 is much smaller compared with the observed value 16.14 e^{2}fm^4 for $B(E2; 1/2^- \rightarrow 3/2^-)$ in ^{7}Li. As in the same way as the case of quadrupole moments, the improved AMD wave function gives the strength of 18.57 e^{2}fm^4 which is as large as the data.

IV. STRUCTURE-CHANGE BETWEEN CLUSTER STRUCTURE AND SHELL-MODEL-LIKE STRUCTURE

In section III we have reported the calculated results and compared them with the experimentally observed values. We have seen that the observed values of various quantities which show interesting dependence on the neutron number are reproduced by AMD qualitatively or excellently as in the case of magnetic moments. It is important to analyze the intrinsic structure of the obtained AMD states in order to understand the fundamental mechanism of such characteristic dependence on the neutron number.

A. Density distribution

The density distributions of the calculated intrinsic states of Li and Be isotopes are shown in the Figs.8 and 9, respectively. In drawing the figures, the density of each intrinsic state is projected onto an adequate plane by integrating out along the axis perpendicular to the plane. We see here systematic but drastic structure-change along the increase of the neutron number. In the results of Li isotopes (Fig.8), it is easily seen that the ^{7}Li system has the largest deformation with a cluster structure. ^{9}Li also has a deformation which is, however, not as large as the one seen in ^{7}Li. ^{11}Li has an almost spherical state that can be expressed by a shell model wave function. In Fig.9 for Be isotopes, more interesting features are seen. In this figure the density distributions of only the normal parity states of Be isotopes are shown except the case of ^{11}Be. Just like the structure-change from ^{7}Li to ^{11}Li, the deformation is most developed in ^{8}Be which has a cluster structure and then gradually decreases toward ^{12}Be which has the most spherical shell-model-like structure. What is novel and interesting in Be is the result that in heavier Be isotopes than ^{12}Be the deformation develops again as the neutron number increases. Rather large deformation is seen in the positive parity state of ^{11}Be which is known to have the ground state with the anomalous positive parity. It is to be noted that deformation has been considered to be one of the essential mechanisms for the decrease of the excitation energy of the $1/2^+$ level in ^{11}Be.

B. Clustering aspect

As mentioned in Sec.I, it is well known that in the $N \approx Z$ region of Li and Be isotopes there appear well-developed cluster structures like the α-α structure of ^{8}Be and the α-t structure of ^{7}Li. Many theoretical studies by the use of the cluster model have been

successfully made both for nuclear structure problems and for nuclear reaction problems. However, there have been very small number of theoretical works which have ascertained the formation of clusters microscopically without assuming the existence of any kinds of clusters. The present AMD theory is a very suitable theoretical framework for the above-mentioned ascertainment.

By checking the spatial centers of Gaussian wave packets given by the values $\{\mathbf{D}\} = \{\mathrm{Re}\mathbf{Z}/\sqrt{\nu}\}$, we have found that the AMD wave functions of ^{7}Li and ^{8}Be have actually the α-t and α-α clustering structure, respectively. Further, the AMD wave function of ^{9}Be has been found to be of the α-α-n structure (or α-^{5}He structure), which has also been well known for a long time as the structure of ^{9}Be.

We are interested in how the clustering structure changes as a function of the neutron number N. In Li isotopes, ^{9}Li has the ^{6}He+t clustering, although it is not so well-developed as the $\alpha + t$ clustering in the ^{7}Li. The heavier nucleus ^{11}Li has no clustering structure.

Figure 10 shows the spatial configuration of the center of each Gaussian wave packet for Be isotopes. The values $\{\mathbf{D}\} = \{\mathrm{Re}\mathbf{Z}/\sqrt{\nu}\}$ are projected to an appropriate plane. The squares and circles correspond to protons and neutrons, respectively. In all Be isotopes, four protons are always grouped spatially into two pairs. Each pair is composed of $p\uparrow$ and $p\downarrow$ and is seen in the figure as just two squares located very closely to each other. The neutrons except for the valence neutron in the even-odd Be isotopes also couple to compose some pairs of $n\uparrow$ and $n\downarrow$. It is shown that many of Be isotopes have two-center clustering structure with at least one α cluster. One will find the $2p+\alpha$ clustering in the positive parity state of ^{6}Be, ^{3}He+α in ^{7}Be, $\alpha+\alpha$ in ^{8}Be, ^{5}He+α in ^{9}Be , ^{6}He+α in ^{10}Be and the ^{7}He+α clustering in the negative parity state of ^{11}Be.

The degree of development of clustering structure is roughly estimated with the relative distances between two pairs of protons which we show in Fig.11. The α clustering is most developed in ^{8}Be and it becomes weaker in heavier isotopes as the neutron number increases. No developed clustering structure is found in ^{12}Be with the neutron magic number $N = 8$. In ^{13}Be and ^{14}Be which have neutron number $N > 8$, the clustering structure develops again. In ^{13}Be, the α is not so normal but is somewhat polarized with neutrons distributed in the outer region. In ^{14}Be, the distortion of α is larger since it is seen that two valence neutrons distribute in the further outer region. In Ref.[30] Be isotopes were studied with the molecular orbital model which describes the Be isotope as composed of an α-α core and surrounding neutrons. It was found there that the inter-α distance decreases when going

from ^{8}Be to ^{12}Be but increases when going from ^{12}Be to ^{14}Be. Since the relative distance between two proton pairs mentioned above is similar to the α-α distance, their results are consistent with ours which have been obtained without any assumption of the existence of clusters.

The calculations of the Extended AMD present us with interesting results about clustering features. In EAMD we have adopted the superposition of two parity-projected Slater determinants which we denote as $|\Phi_1^{\pm}(\mathbf{Z})\rangle$ and $|\Phi_2^{\pm}(\mathbf{Z}')\rangle$. In most of normal parity states of Be isotopes, the main component $|\Phi_1^{\pm}(\mathbf{Z})\rangle$ has proved to be almost the same as the wave function of the simple AMD calculation. The minor component $|\Phi_2^{\pm}(\mathbf{Z}')\rangle$ mixes in with only small amount and gives an improvement for the description of the system with the major component. By analyzing $\{\mathbf{Z}'\}$ in the minor component $|\Phi_2^{\pm}(\mathbf{Z}')\rangle$, we have found that the types of improvement made by $|\Phi_2^{\pm}(\mathbf{Z}')\rangle$ can be classified into three types. The first type is seen in the cases of ^{6}Be and ^{7}Be. The state $|\Phi_1^{\pm}(\mathbf{Z})\rangle$ in ^{7}Be (^{6}Be), has the same clustering configuration ^{3}He+α ($2p+\alpha$) but with larger inter-cluster distance compared to the one in the simple AMD result. On the other hand, $\{\mathbf{Z}_i'\}$ in $|\Phi_2^{\pm}(\mathbf{Z}')\rangle$ are distributed between the two clusters so that the spatial region between the two clusters does not become too low in density.

The second type of the improvement is concerned with the relative wave function between the clusters. In ^{5}Be (^{9}Be), the state $|\Phi_1^{\pm}(\mathbf{Z})\rangle$ is found to have the same $\alpha+\alpha$ (^{5}He+α) clustering structure as the one obtained by simple AMD. The second component $|\Phi_2^{\pm}(\mathbf{Z}')\rangle$ has the same clustering configuration, but its inter-cluster distance is larger by about 2 fm than the inter-cluster distance of $|\Phi_1^{\pm}(\mathbf{Z})\rangle$. The total wave function $|\Phi_1^{\pm}(\mathbf{Z})\rangle$+$|\Phi_2^{\pm}(\mathbf{Z}')\rangle$ results in improving the outer tail of the wave function of the relative motion between the clusters. In heavier Be isotopes, we observe the third type of improvement by the minor component $|\Phi_2^{\pm}(\mathbf{Z}')\rangle$. In this case, $|\Phi_1^{\pm}(\mathbf{Z})\rangle$+$|\Phi_2^{\pm}(\mathbf{Z}')\rangle$ represents the mixing of two different channels of clustering. In ^{10}Be, ^{11}Be and ^{12}Be, the main component $|\Phi_1^{\pm}(\mathbf{Z})\rangle$ represents the ^{6}He+α, ^{7}He+α and ^{8}He+α channels and the minor component $|\Phi_2^{\pm}(\mathbf{Z}')\rangle$ corresponds to the ^{5}He+^{5}He, ^{6}He+^{5}He and ^{6}He+^{6}He channels, respectively. In ^{13}Be, the main component $|\Phi_1^{\pm}(\mathbf{Z})\rangle$ has the ^{8}He+^{5}He configuration with the polarized ^{5}He, while the minor component $|\Phi_2^{\pm}(\mathbf{Z}')\rangle$ has ^{8}He+$\alpha+n$ structure with the valence neutron locating far from the center of the nucleus.

More interesting aspect of clustering is found in the non-normal parity state of ^{11}Be. Figure 12 shows the spatial configurations of $\{\mathrm{Re}\mathbf{Z}/\sqrt{\nu}\}$ in $|\Phi_1^{\pm}(\mathbf{Z})\rangle$ and $\{\mathrm{Re}\mathbf{Z}'/\sqrt{\nu}\}$ in

$|\Phi_2^{\pm}(\mathbf{Z}')\rangle$ comparing with the result of simple AMD. The positive parity state obtained with the simple AMD has the ^{7}He+α clustering feature (seen in Fig.12-a). On the other hand the EAMD calculation gives the state with a mixture of α+^{6}He+n and ^{5}He+^{6}He configurations. Both configurations in the EAMD calculation differ from the one in the AMD calculation, and they describe the behavior of the valence neutron far from the center better than the simple AMD calculation.

Though the two states $|\Phi_1^{\pm}\rangle$ and $|\Phi_2^{\pm}\rangle$ are not orthogonal to each other, in most Be isotopes it is found that the second state $|\Phi_2^{\pm}\rangle$ has a significant component orthogonal to $|\Phi_1^{\pm}\rangle$. In the total wave function, $|\Phi_1^{\pm}\rangle$+$|\Phi_2^{\pm}\rangle$, the orthogonal component to $|\Phi_1^{\pm}\rangle$ is about 10 %. In Table III we show the percentage of the normalized component $|\Phi_1^{\pm}\rangle^N \equiv |\Phi_1^{\pm}\rangle/\||\Phi_1^{\pm}\rangle\|$ contained in the normalized total wave function $|(\Phi_1^{\pm}+\Phi_2^{\pm})\rangle^N \equiv (|\Phi_1^{\pm}\rangle+|\Phi_2^{\pm}\rangle)/\|(|\Phi_1^{\pm}\rangle+|\Phi_2^{\mp}\rangle)\|$, $|^N\langle\Phi_1^{\pm}|(\Phi_1^{\pm}+\Phi_2^{\pm})\rangle^N|^2$. The above-mentioned fact that the main component $|\Phi_1^{\pm}\rangle$ is very similar to the wave function of the simple AMD calculation which adopts one parity-projected Slater determinant and that the second component $|\Phi_2^{\pm}\rangle$ mixes in with a small mixing amplitude implies that the AMD study adopting only one parity-projected Slater determinant is usually sufficiently reliable.

C. Indispensable role of parity projection in describing asymmetric cluster structure

We here point out that the parity projection is essential for describing the precise structure especially concerning with the clustering aspects. As shown above, $\alpha+t$ clustering in ^{7}Li is described by the variational calculation by the use of the parity projected AMD wave function. However when we have adopted the variational calculation without the parity projection we have obtained the state not with the $\alpha+t$ clustering configuration but with $t+n+t$ clustering. The AMD wave function without parity projection is given by a single Slater determinant, and its variational calculation is considered to be one of approximated frameworks of the Hatree-Fock method. In any Hartree-Fock type theory which adopts a single Slater determinant, the description of the $\alpha+t$ clustering can be made only by a parity-violating intrinsic state. But, usually the minimum energy is obtained not by parity-violating configuration but by parity-conserving configuration. This is the reason why we have failed to obtain the asymmetric configuration of $\alpha+t$ but have obtained the symmetric configuration of $t+n+t$ in ^{7}Li in the AMD calculation without parity projection. We have encountered the same situation in the study of ^{20}Ne [27]. By the AMD calculation with par-

ity projection, we could confirm the existence of α+^{16}O clustering in ^{20}Ne. However, when we made the AMD calculation without parity projection, we never obtained the asymmetric (parity-violating) α+^{16}O clustering configuration but a symmetric (parity-conserving) configuration. Therefore we stress here that the parity projection is important to describe the structure of light nuclei and it is sometimes dangerous to extract a conclusion with the framework in which the functional space is restricted within a single Slater determinant without parity projection.

D. Correlations of the structure change with the observed electromagnetic properties

The drastic change of the intrinsic structure has been discussed in the previous subsections A and B. Our aim here is to understand the fundamental mechanism how the observed electromagnetic properties reflect the systematical structure change. Furthermore we aim to find what information about the nuclear structure can be given by the observed data.

The observed magnetic moments of Li isotopes change systematically as the neutron number N changes. The shift of the ^{7}Li magnetic moment from the Schmidt value 3.79 n.m. of the $0p_{3/2}$ proton orbit has been considered to be closely related with the clustering structure. Below we discuss this point on the basis of our AMD calculations. An important point of the AMD results which we need to remember in the following discussions is that neutrons make no contribution to the calculated magnetic moments. This result is because of the property of the calculated AMD wave functions of Li isotopes that neutrons are all paired off, namely every spin-up neutron wave packet always shares the same spatial point with a spin-down neutron wave packet. It implies that the total intrinsic spin of neutrons is zero and the total angular momentum of neutrons is exhausted by the total orbital angular momentum.

In the following discussions, one should recall that the clustering gives two kinds of fundamental effects on the nuclear structure. One is caused by the spatial relative distance between clusters (spatial clustering), and the other is concerned with the angular momentum coupling of nucleons caused by the clustering correlation of nucleons (cluster coupling of angular momenta). A typical example of the latter kind is found in the so-called shell-model cluster which is the cluster appearing in the SU_3 coupling shell model configuration. According to the Bayman-Bohr theorem [40], the clustering wave function with the minimum spatial separation of clusters is equivalent to the the SU_3-shell-model wave function. As

we see below, the effect of clustering on the magnetic moment is not due to the spatial clustering but due to the cluster coupling of angular momenta. In order to extract the effect of the cluster coupling of angular momenta from our AMD wave functions, we have artificially made the inter-cluster relative distance in the AMD wave function small so as to get shell-model limit state. In practice we have transformed all the parameters $\mathbf{Z}_i$ as $\{\mathbf{Z}\} \rightarrow \{a\mathbf{Z}\}$ where a is a real constant that is sufficiently small. It should be noted that this transformation does not largely affect the internal wave functions of clusters contained in the AMD wave functions, because nucleons inside each cluster are located closely each other. The state obtained in the shell model limit does not have the developed clustering in view of the inter-cluster relative distance any more, but keeps the angular momentum coupling correlation caused by the clustering structure of the original AMD wave function. Table IV shows some electromagnetic quantities calculated with the angular-momentum-projected states from the shell-model-limit intrinsic state mentioned above, which are compared with the original AMD calculations. In Table IV we have also shown the expectation values of squared total angular momenta of protons $\langle \mathbf{J}_p^2 \rangle$ and neutrons $\langle \mathbf{J}_n^2 \rangle$ and those of squared total orbital angular momentum of protons $\langle \mathbf{L}_p^2 \rangle$. We see that the magnetic dipole moments in the shell model limit are almost the same as the original AMD and reproduce the experimental data. Furthermore we see that the values of $\langle \mathbf{J}_p^2 \rangle$, $\langle \mathbf{J}_n^2 \rangle$, and $\langle \mathbf{L}_p^2 \rangle$ in the shell model limit are close to those of the original AMD. These results given in Table IV confirm that the angular momentum coupling of nucleons in the shell-model-limit wave functions is similar to the one in the original AMD wave functions, and that the magnetic moments are not sensitive to the spatial clustering but to the cluster coupling of angular momenta. Below we explain the characters of the angular momentum coupling of nucleons in the shell-model-limit wave functions. These characters are of course different from those of the j-j coupling shell model wave functions when the original AMD wave functions have clustering structure.

In Li isotopes, the magnetic dipole moments in the shell model limit are determined by the orbit of only the third valence proton in $0p$ orbits. In ^{11}Li with the closed shell for neutron orbits, $\langle \mathbf{J}_p^2 \rangle$ is 3.75 ($= 3/2(3/2 + 1)$) and $\langle \mathbf{J}_n^2 \rangle$ is 0 in the shell model limit. This is because the angular momenta of all neutrons couple totally to 0 and only the $0p_{3/2}$ orbit is allowed for the the valence proton orbits in the ground state with total spin 3/2. In this case the magnetic moment μ is as large as the Schmidt value. In ^{7}Li, the magnitude 2.61 of $\langle \mathbf{J}_n^2 \rangle$ implies that the component with the non-zero total angular momentum of neutrons is considerably large. It is to be noted that, as we mentioned before, the total angular

momentum of neutrons is equal to the total orbital angular momentum of neutrons. The magnitude 3.12 of $\langle J_p^2 \rangle$ which is smaller than 3.75 is due to the mixing of $0p_{3/2}$ with $0p_{1/2}$, and this proton angular momentum couples with the non-zero angular momentum of neutrons so as to compose totally 3/2 spin. This $0p_{1/2}$ mixing in proton orbits reduces the μ value from the Schmidt value. ^{9}Li has the medium properties between ^{11}Li and ^{7}Li. In Table IV we see that the $0p_{1/2}$ mixing of proton in ^{9}Li is smaller than in ^{7}Li but is larger than in ^{11}Li and also that the total angular momentum of neutrons in ^{9}Li is smaller than in ^{7}Li but is larger than in ^{11}Li.

In summary, it is concluded that the dependence of the μ-moments of Li isotopes on the neutron number N originates from the angular momentum coupling correlation caused by the clustering structure. Our results shows that the magnetic moments is not sensitive to the relative distance between clusters and that the observed data gives little information about the detail of the inter-cluster relative motion.

In contrast to dipole moments, electric quadrupole moments are sensitive to the relative distance between clusters. In the following discussion of the N-dependence of the electric quadrupole moments, we try to decompose the calculated Q-moments into two components: the first component is due to the spatial clustering and the second component is due to the other properties of the AMD wave function including the cluster coupling of angular momenta. We regard that the second components are given by the Q-moments calculated by the shell-model-limit wave functions defined above. They are shown in Table IV together with the Q-moments of the AMD calculation and are -15.1, -23.28 and -29.41 e·mb for ^{7}Li, ^{9}Li and ^{11}Li, respectively. These values show that the second component becomes smaller as the neutron number N decreases. Such N-dependence can be explained by the argument similar to that made for μ-moments about the mixture of proton's $0p_{1/2}$ and $0p_{3/2}$ orbits. The mixing of the $0p_{1/2}$ proton configuration into the $0p_{3/2}$ proton configuration is larger for smaller N. It makes the Q-moment smaller for smaller N because of the fact $\langle 0p_{1/2}|Q^{\rm op}|0p_{1/2}\rangle = 0$ with $Q^{\rm op}$ standing for the Q-moment operator which is a tensor operator with rank two. By subtracting this component from the total Q-moments (namely the Q-moments of the AMD calculation), we obtain the first component which is due to the spatial clustering. The first component becomes smaller as the neutron number increases from ^{7}Li to ^{11}Li. Such dependence of the first component on the neutron number is consistent with the drastic change of clustering structure. Thus the systematical experimental data are qualitatively explained by the structure change seen in our AMD results. The AMD value of the ^{7}Li

Q-moment given in Table IV is not the value obtained by improving the α-t relative wave function mentioned in Sec.III-D but the value obtained by using single parity-projected AMD Slater determinant. Yet the first component of the Q-moment is largest for ^{7}Li than for ^{9}Li and ^{11}Li.

Finally we analyze the AMD wave functions by calculating the total number of the oscillator quanta. The state with clustering structure usually contains large amount of the high-lying shell-model orbits and gives larger expectation value of the total number of the oscillator quanta than the state with the shell-model-like structure. Our analysis is made separately for the neutron and proton orbits. We introduce the value ΔN_p and ΔN_n which stand for the deviation of the proton and neutron orbits in the AMD wave function from those in the simple shell-model wave function;

$$\Delta N_p \equiv \frac{\langle P^J_{MK}\Phi^{\pm}|N_p^{\rm op}|P^J_{MK}\Phi^{\pm}\rangle}{\langle P^J_{MK}\Phi^{\pm}|P^J_{MK}\Phi^{\pm}\rangle} - N_p^{\rm min},$$

$$\Delta N_n \equiv \frac{\langle P^J_{MK}\Phi^{\pm}|N_n^{\rm op}|P^J_{MK}\Phi^{\pm}\rangle}{\langle P^J_{MK}\Phi^{\pm}|P^J_{MK}\Phi^{\pm}\rangle} - N_n^{\rm min},$$

where $N_p^{\rm op}$ and $N_n^{\rm op}$ are the oscillator quantum number operators and $N_p^{\rm min}$ and $N_n^{\rm min}$ are the minimum oscillator quantum numbers given by the simple shell model for protons and neutrons, respectively. The state with shell-model-like structure should have small ΔN values, while the state with well-developed clustering structure should have large values of ΔN. Figure 13 shows ΔN_p and ΔN_n of Be and Li isotopes. For both Li and Be, ΔN_n is quite large with the neutron number $N = 4$ and it decreases as N increases. ΔN_n has the smallest value 0 in the nuclei with neutron magic number $N = 8$, and it increases again as N increases in the region with $N \geq 8$. Such neutron-number dependence of ΔN_n directly reflects the shell effect of neutron orbits. We see that the ΔN_p for proton orbits has almost the same dependence on the neutron number N. A very interesting fact is that the shell effect of neutron orbits is reflected on the proton orbits which have close relation to the electric and magnetic properties. What causes the clustering structure is such feature that protons behave accompanying the neutrons orbits. This feature is fundamental for the mechanism of the N-dependence of the electromagnetic data.

V. SUMMARY

Structure of odd-even and even-even Li and Be isotopes have been studied with AMD (antisymmetrized molecular dynamics). Energy spectra and other quantities have been reproduced well. AMD is the first framework which has succeeded in reproducing systematical data of electric and magnetic properties such as magnetic dipole moments and electric quadrupole moments in wide range of light isotopes. In our AMD framework we never need to introduce the effective charge but we use only the bare charge. It is because the drastic change of proton orbits from clustering structure to the shell-model-like structure is described automatically by the AMD wave function.

It has been ascertained that the well-developed clustering structure appears in ^{7}Li and ^{8}Be without assuming the existence of any kind of clusters. The clustering structure seen in the $N \approx Z$ region of Li and Be isotopes gets weaker as the neutron number N increases, and changes toward the shell-model-like structure in ^{11}Li and ^{12}Be with the neutron magic number $N = 8$. It is suggested that possible clustering aspects appear again in neutron-richer region like ^{14}Be. Thus the drastic structure change as a function of the neutron number N has been explained in connection with the shell effect of neutron orbits.

N-dependence of electric and magnetic data has been discussed in relation with the structure change. It has been shown that systematical data of Li isotopes directly reflect the drastic structure change between clustering structure and shell-model-like structure. Strictly speaking, N-dependence of μ-moments has been explained in terms of the cluster coupling of angular momenta, namely the angular momentum coupling correlation of nucleons which is caused by clustering structure. In the case of Q-moments which are more sensitive to the nuclear deformation, N-dependence has been explained in terms of two effects of clustering structure; one is the spatial clustering and the other is the cluster coupling of angular momenta.

We have also tried to make Extended AMD calculations with a superposition of two parity-projected Slater determinants for Be isotopes. It has been found that in most cases the first Slater determinant which is the major component is almost the same as the wave function of the simple AMD calculation and the second Slater determinant which is the minor component is not so large and gives an improvement for the description of the system with the major component. Therefore the AMD calculation by the use of single parity-projected Slater determinant is approved to be sufficient for describing leading properties of nuclear

structure. In some nuclei, however, two Slater determinants have been found to describe two channels of different clustering configurations.

In some cases, further improvements of AMD wave functions have been found to be important. For example, the improved AMD calculation which adopts a superposition of several Slater determinants has proved to be necessary for the $J^{\pi} = 1/2^{+}$ state in ^{11}Be in order to describe the behavior of the valence neutron better than the simple AMD and also in order to give better results about the energy and radius, even though the reproduction is not sufficient yet. We have shown that a superposition of several AMD wave functions reproduces the long tail of the wave function in two cases, the neutron halo in ^{11}Be and the α+t relative motion of ^{7}Li.

We have found that the density dependence of the effective interaction plays important roles in getting better agreements with data of radii, electric quadrupole moments, and low excitation energies of non-normal parity states. These quantities are sensitive to the density distribution. Our results show that the density dependence of the effective interaction is indispensable in obtaining better reproduction of density distributions in a wide range of isotopes.

It is expected that many kinds of interesting structure exist in excited states of neutron-rich nuclei. Though some low excited states have been described by angular momentum projection from the intrinsic state obtained with AMD, the detailed structure of excited states are to be studied by using the constrained frictional cooling method in the AMD approach. Such kind of study has been already made in ^{20}Ne for the investigation of the structure change in yrast states [27].

Acknowledgement

The authors would like to thank Professor D. Brink for helpful discussions and encouragements. Helpful comments of Professor I. Tanihata are also gratefully acknowledged. They are also grateful to Professor K. Asahi, Dr. H. Okuno, and other experimentalists for valuable comments and discussions. Their thanks are also due to Professors D. Baye for helpful discussions during his stay in Kyoto. They also would like to thank Drs. A. Ohnishi and T. Maruyama for many discussions at the early stage of this work.

Table I

The adopted width parameters ν of Be and Li isotopes in the AMD calculations. They are chosen so as to make the energies minumum.

	$t_3 = 0$ MeV $m = 0.56$ (fm^{-2})	$t_3 = 4000$ MeV $m = 0.576$ (fm^{-2})
^{6}Be(+)	0.215	0.195
^{7}Be(−)	0.230	0.200
^{8}Be(+)	0.250	0.205
^{9}Be(−)	0.245	0.195
^{9}Be(+)	0.235	0.200
^{10}Be(+)	0.230	0.190
^{10}Be(−)	0.225	0.190
^{11}Be(−)	0.220	0.180
^{11}Be(+)	0.220	0.180
^{12}Be(+)	0.215	0.175
^{12}Be(−)	0.210	0.180
^{13}Be(+)	0.205	0.170
^{14}Be(+)	0.210	0.170
^{7}Li(−)	0.230	0.200
^{9}Li(+)	0.210	0.180
^{11}Li(+)	0.195	0.170

Table II

The $E2$ transition strength $B(E2; I_1 \to I_2)$. The theoretical values are the AMD results calculated with the interaction parameters $m = 0.576$ and $t = 4000$MeV. In ^{7}Li the strength $B(E2; 1/2^- \to 3/2^-)$ calculated with the improved AMD wave function is shown in the parenthesis.

	$B(E2)$			
	TRANSITION ($I_1 \to I_2$)	ENERGY (MeV)	EXP. ($\mathrm{e}^2\mathrm{fm}^4$)	THEORY ($\mathrm{e}^2\mathrm{fm}^4$)
^{7} Li	$1/2^- \to 3/2^-$	0.48→ 0	16.14	7.51 (18.57)
	$7/2^- \to 3/2^-$	4.63→ 0	3.51	4.72
^{9} Be	$5/2^- \to 3/2^-$	2.43→ 0	27.8	18.35
	$7/2^- \to 3/2^-$	6.76→ 0	7.24	7.73
^{10} Be	$2^+ \to 0^+$	3.37 → 0	10.49	9.46

Table III

Percentage of the normalized compornent $|\Phi_1\rangle^N \equiv |\Phi_1\rangle/|||\Phi_1\rangle||$ contained in the normalized total wave function $|(\Phi_1 + \Phi_2)\rangle^N \equiv (|\Phi_1\rangle + |\Phi_2\rangle)/|||\Phi_1\rangle + |\Phi_2\rangle||$.

	$\lvert{}^N\langle\Phi_1\rvert(\Phi_1 + \Phi_2)\rangle^N\rvert^2$
^{6}Be(+)	0.83
^{7}Be(−)	0.84
^{8}Be(+)	0.83
^{9}Be(−)	0.90
^{10}Be(+)	0.85
^{11}Be(−)	0.96
^{11}Be(+)	0.88
^{12}Be(+)	0.96
^{13}Be(+)	0.90

Table IV

Comparison of various quantities calculated with the AMD wave functions to those calculated with the shell-model-limit wave functions of AMD. The notations, $\langle \mathbf{J}_p^2 \rangle$, $\langle \mathbf{J}_n^2 \rangle$ and $\langle \mathbf{L}_p^2 \rangle$ are explained in the text. The experimental data of the magnetic dipole moments μ and the electric quadrupole moments Q are also shown for comparison. The expectation values are calculated with the total angular momentum projected states. The adopted interaction parameters are $m = 0.576$ and $t = 4000$ MeV.

		μ (n.m.)	Q (e·mb)	$< \mathbf{J}_p^2 >$	$< \mathbf{J}_n^2 >$	$< \mathbf{L}_p^2 >$
^{7}Li	EXP.	3.27	-40(3)	–	–	–
	AMD	3.15	-27.6	3.31	2.74	2.17
	shell model limit	3.14	-15.1	3.12	2.61	2.00
^{9}Li	EXP.	3.44	-27(1)	–	–	–
	AMD	3.52	-26.6	3.54	1.07	2.01
	shell model limit	3.53	-23.3	3.54	1.02	2.00
^{11}Li	EXP.	3.76	-31(5)	–	–	–
	AMD	3.79	-29.4	3.75	0.02	2.00
	shell model limit	3.79	-29.4	3.75	0.00	2.00

REFERENCES

1. *Proc. VI Int. Conf. on Nuclei Far from Stability and IX Int. Conf. on Atomic Masses and Fundamental Constants*, Bernkastel-Kues (1992), eds. R. Neugart and A. Wöhr, *Institute of Physics Conference Series* **No. 132** (1993).

2. *Proc. II Int. Conf. on Radioactive Nuclear Beams*, Louvain-la Neuve (1991), ed. Th Delbar (IOP Publishing, London, 1992).

3. *Proc. IV Int. Conf. on Nucleus-Nucleus Collisions* , Kanazawa (1991), eds. H. Toki, I. Tanihata, and H. Kamitsubo, Nucl. Phys. **A538** (North Holland, 1992).

4. *Proc. Int. Symp. on Structure and Reactions of Unstable Nuclei*, Niigata (1991), eds. K. Ikeda and Y. Suzuki, (World Scientific, 1992).

5. M. V. Zhukov, B. V. Danilin, D. V. Fedorov, J. M. Bang, I. J. Thompson, and J. S. Vaagen, Phys. Report **231**, No.4, 151 (1993); K. Ikeda, Nucl. Phys. **A538**, 355c (1992).

6. I. Tanihata, H. Hamagaki, O. Hashimoto, S. Nagamiya, Y. Shida, N. Yoshikawa, O. Yamakawa, K. Sugimoto, T. Kobayashi, D. E. Greiner, N. Takahashi, and Y. Nojiri, Phys. Lett. **B160**, 380 (1985); I. Tanihata, H. Hamagaki, O. Hashimoto, Y. Shida, N. Yoshikawa, K. Sugimoto, O. Yamakawa, T. Kobayashi, and N. Takahashi, Phys. Rev. Lett. **55**, 2676 (1985); I. Tanihata, T. Kobayashi, O. Yamakawa, S. Shimoura, K. Ekuni, K. Sugimoto, N. Takahashi, T. Shimoda, and H. Sato, Phys. Lett. **B206**, 592 (1988).

7. W. Mittig, J. M. Chouvel, Zhang Wen Long, L. Bianchi, A. Cunsolo, B. Fernandez, A. Foti, J. Gastebois, A. Gillebert, C. Gregoire, Y. Schutz, and C. Stephan, Phys. Rev. Lett. **59**, 1889 (1987); M. G. Saint-Laurent, R. Anne, D. Bazin, D. Guillemaud-Mueller, U. Jahnke, Jin Gen Ming, A. C. Mueller, J. F. Bruandet, F. Glasser, S. Kox, E. Liatard, Tsan Ung Chan, G. J. Costa, C. Heitz, Y. El-Masri, F. Hanappe, R. Bimbot, E. Arnold, and R. Neugart, Z. Phys. **A332**, 457 (1989).

8. T. Kobayashi, O. Yamakawa, K. Omata, K. Sugimoto, T. Shimoda, N. Takahashi, and I. Tanihata, Phys. Rev. Lett. **60**, 2599 (1988); R. Anne, S. E. Arnell, R. Bimbot, H. Emling, D. Guillemaud-Mueller, P. G. Hansen, L. Johannsen, B. Jonson, M. Lewitowitz, S. Mattsson, A. C. Mueller, R. Neugart, G. Nyman, F. Pougheon, A. Richter, K. Riisager, M. G. Saint-Laurent, G. Schrieder, O. Sorlin, and K. Wilhelmsen,

Phys. Lett. **B250**, 19 (1990); M. Fukuda, T. Ichihara, N. Inabe, T. Kubo, H. Kumagai, T. Nakagawa, Y. Yano, I. Tanihata, M. Adachi, K. Asahi, M. Kouguchi, M. Ishihara, H. Sagawa, and T. Shimoura, Phys. Lett. **B268**, 339 (1991).

9. T. Otsuka, N. Fukunishi, and H. Sagawa, Phys. Rev. Lett. **70**, 1385 (1993).

10. K. Ikeda, H. Horiuchi, S. Saito, Y. Fujiwara, M. Kamimura, K. Kato, Y. Suzuki, E. Uegaki, H. Furutani, H. Kanada, T. Kaneko, S. Nagata, H. Nishioka, S. Okabe, T. Sakuda, M. Seya, Y. Abe, Y. Kondo, T. Matsuse, and A. Tohsaki- Suzuki, *Comprehensive Study of Structure of Light Nuclei*, Prog. Theor. Phys. Suppl. **68**. (1980)

11. A. Arima, *Nuclear Cluster Correlation, Heavy Ion Collisions*, **Vol. 1**, Chapt.3 , ed. R. Bock, (North Holland, Amsterdam, 1979), pp.417 $\sim$ 483.

12. Y. C. Tang, *Microscopic Description of the Nuclear Cluster Theory, Lecture Notes in Physics* **145**, (Springer, Berlin, 1981)

13. V. I. Kukulin, V. G. Neudatchin, I. T. Obukhovski, and Yu. F. Smirnov, *Clusters as Subsystems in Light Nuclei*, (*Clustering Phenomena in Nuclei* **Vol.3**, Vieweg, Braunschweig, 1982), pp.1 $\sim$ 155.

14. H. Horiuchi and K. Ikeda, *Cluster Model of the Nucleus, International Review of Nuclear Physics* **Vol.4**, eds. T. T. S. Kuo, and E. Osnes, (World Scientific, Singapore, 1985), pp.1 $\sim$ 258.

15. H. Horiuchi, Nucl. Phys. **A522**(1991), 257c.

16. H. Horiuchi, T. Maruyama, A. Ohnishi, and S. Yamaguchi, *Proc. Int. Conf. on Nuclear and Atomic Clusters*, Turku (1991), eds. M. Brenner, T. Lönnroth, and F. B. Malik, (Springer, 1992), p.512; *Proc. Int. Symp. on Structure and Reactions of Unstable Nuclei*, Niigata (1991), eds. K. Ikeda and Y. Suzuki, (World Scientific, 1992), p.108.

17. H. Horiuchi, A. Ono, Y. Kanada, T. Maruyama, and A. Ohnishi, *Proc. First Joint Italian-Japanese Meeting within the INFN-RIKEN Agreement on Perspectives in Heavy Ion Physics*, Catania (1992), eds. M. Di Toro and E. Migneco, *Italian Physical Society Conference Proceedings* **Vol. 38** (1993), p.223.

18. A. Ono, H. Horiuchi, T. Maruyama, and A. Ohnishi, Phys. Rev. Letters **68** (1992), 2898.

19. A. Ono, H. Horiuchi, T. Maruyama, and A. Ohnishi, Prog. Theor. Phys. **87** (1992), 1185.

20. A. Ono, H. Horiuchi, T. Maruyama, and A. Ohnishi, Phys. Rev. **C47** (1993), 2652.

21. A. Ono, H. Horiuchi, and T. Maruyama, Phys. Rev. **C48** (1993), 2946.

22. A. Ono and H. Horiuchi, to be published in Phys. Rev. **C**.

23. H. Horiuchi, *Proc. NATO Advanced Study Institute on Hot and Dense Nuclear Matter*, Bodrum (1993), eds. W. Greiner, H. Stöcker, and A. Gallmann, (Plenum, 1994), p.215.

24. H. Horiuchi, to appear in *Proc. Fifth Int. Conf. on Nucleus-Nucleus Collisions*, Taormina (1994).

25. H. Horiuchi, A. Ono, and Y. Kanada-En'yo, *Proc. Seventh Int. Conf. on Nuclear Reaction Mechanisms*, Varenna (1994), ed. E. Gadioli, p.421.

26. H. Horiuchi, Y. Kanada-En'yo, and A. Ono, *Proc. Second Int. Conf. on Atomic and Nuclear Clusters*, Santorini (1993), eds. G. S. Anagnostatos and W. von Oertzen, Z. Phys. **A349**, 279 (1994).

27. Y. Kanada-En'yo and H. Horiuchi, Prog. Theor. Phys. **93** No.1 (1995).

28. G.F.Bertsch and S.Das Gupta, Phys.Rep. **160** (1988),189.

29. J. Aichelin, Phys. Reports **202**, 233 (1991).

30. M. Seya, M. Kohno, and S. Nagata, Prog. Theor. Phys. **65** (1981), 204.

31. H. Feldmeier, Nucl. Phys. **A515**, 147 (1990); *Proc. NATO Advanced Study Institute on the Nuclear Equation of State*, Peñiscola(1989), eds. W. Greiner and H. Stöcker, (Plenum, 1989), p.375.

32. D. M. Brink, *Proc. Int. School of Phys. "Enrico Fermi"*, **course 36** (1965), ed. C. Bloch, p.247.

33. S. Drożdż, J. Okolowcz, and M. Ploszajczak, Phys. Lett. **109B**, 145 (1982); E. Caurier, B. Grammaticos and T. Sami, Phys. Lett. **109B**, 150 (1982); W. Bauhoff, E. Caurier, B. Grammaticos and M. Ploszajczak, Phys. Rev. **C32**, 1915 (1985).

34. A. B. Volkov, Nucl. Phys. **74** (1965), 33.

35. N. Yamaguchi, T. Kasahara, S. Nagata, and Y. Akaishi, Prog. Theor. Phys. **62** (1979), 1018;
R. Tamagaki, Prog. Theor. Phys. **39** (1968), 91.

36. T. Ando, K.Ikeda, and A. Tohsaki, Prog. Theor. Phys. **64**, 1608 (1980).

37. P. Raghavan, At. Data Nucl. Data Tables **42**, 189 (1989).

38. E. Arnold, J. Bonn, R. Gegenwart, W. Neu, R. Neugart, E.-W. Otten, G. Ulm, K. Wendt, and ISOLDE Collaboration, Phys. Lett. **B197**, 311 (1987).

39. E. Arnold, J. Bonn, W. Neu, R. Neugart, E.W. Otten, the ISOLDE Collaboration, Z. Phys. **A331**, 295 (1988); E. Arnold, J. Bonn, A. Klein, R. Neugart, M. Neuroth, E.W. Otten, P. Lievens, H. Reich, W. Widdra, and ISOLDE Collaboration, Phys. Lett. **B281**, 16 (1992).

40. B. F. Bayman and A. Bohr, Nucl. Phys. **9**, 596 (1958/59).

FIGURE CAPTIONS

Fig.1 Binding energies of Li and Be isotopes calculated with the Volkov force No.1 (m=0.56) (a) and the MV1 force (m=0.576) (b). Experimental data are also shown.

Fig.2 Energy spectra of ^{7}Li and ^{9}Li calculated with the Volkov force No.1 (m=0.56) (a) and the MV1 force (m=0.576) (b). Observed spectra are also shown.

Fig.3 Energy spectra of Be isotopes. Calculated results with the Volkov force No.1 (m=0.56) (a) and the MV1 force (m=0.576) (b) are shown and compared with experimental data.

Fig.4 Root mean square radii of Li and Be isotopes. They are calculated with AMD and EAMD using the interaction Volkov force No.1 (m=0.56) (a) and MV1 force (m=0.576) (b). Squares represent the interaction radii derived from the data of interaction cross sections [6].

Fig.5 Density of the positive parity state of ^{11}Be calculated by superposing several Gaussians for the last valence neutron wave function. The solid (dashed) curve shows neutron (proton) density.

Fig.6 Magnetic dipole moments. The triangle shows the magnetic moment of another nearly degenerate AMD state. Observed data are shown with squares [37,38].

Fig.7 Electric quadrupole moments calculated with the MV1 force (m=0.576) (triangles). A circle is the moment of ^{7}Li calculated with the improved AMD with the same interaction. They are compared with experimental data (squares) [37,39].

Fig.8 Matter density distribution of AMD states of Li isotopes. The intrinsic densities before parity projection are shown. Density is projected to a x-y plane and integrated along the z-axis perpendicular to the plane. Units of x- and y-axes are in fm.

Fig.9 Matter density distribution of AMD states of Be isotopes. The intrinsic densities before parity projection are shown. Density is projected to a x-y plane and integrated along the z-axis perpendicular to the plane. Units of x- and y-axes are in fm.

Fig.10 Spatial configurations of the centers of nucleon wave packets in normal parity states of Be isotopes. $\{Re\mathbf{Z}/\sqrt{\nu}\}$ in AMD are projected to an adequate plane. Circles and squares with up arrow (down arrow) represent the centers of $n\uparrow$ ($\downarrow$) and $p\uparrow$ ($\downarrow$), respectively.

Fig.11 Mass number A dependence of the relative distance between two proton pairs of normal

and non-normal parity intrinsic states in Be isotopes. Solid line is for normal parity states and dashed line for non-normal parity states.

Fig.12 Spatial configurations for the positive parity state of ^{11}Be. Figure (a) shows $\{\mathrm{Re}\mathbf{Z}/\sqrt{\nu}\}$ of the AMD wave function. Figure (b) shows $\{\mathrm{Re}\mathbf{Z}/\sqrt{\nu}\}$ in Φ_1 (b-1) and $\{\mathrm{Re}\mathbf{Z}'/\sqrt{\nu}\}$ in Φ_2 (b-2) obtained with EAMD. Circles and squares with up arrow (down arrow) correspond to the centers of $n\uparrow(\downarrow)$ and $p\uparrow(\downarrow)$, respectively.

Fig.13 Deviation of the total number of oscillator quanta of the AMD state from that of the simple shell-model wave function. Deviation for proton and neutron orbits is shown as $\Delta\mathrm{N}_p$ and $\Delta\mathrm{N}_n$ which are defined in the text.

Fig.1

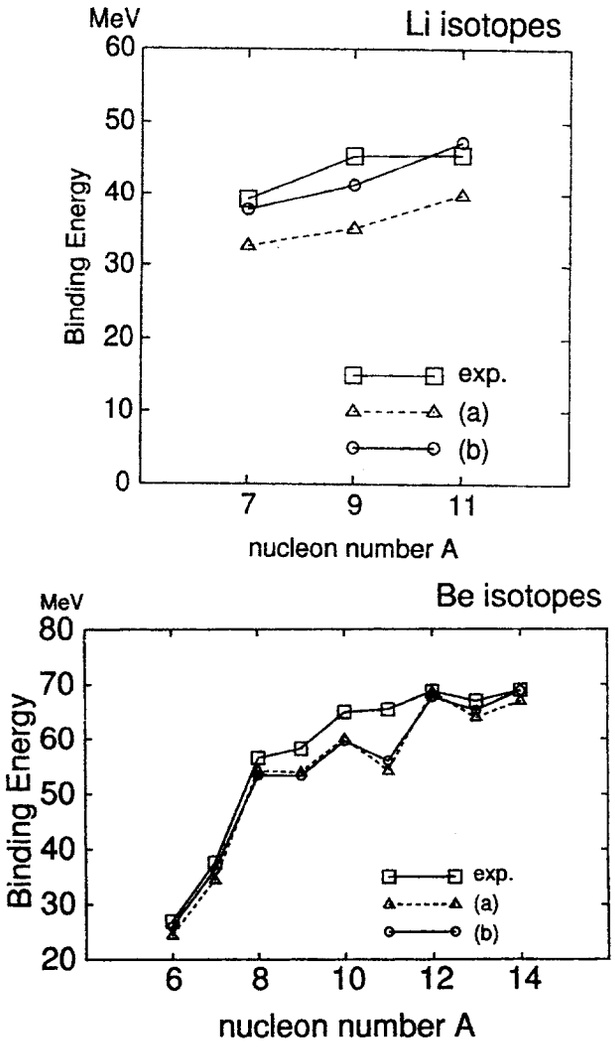
MeV
Li isotopes
60
50
40
30
20
10
0
Binding Energy
7
9
11
nucleon number A
exp.
(a)
(b)
MeV
Be isotopes
80
70
60
50
40
30
20
Binding Energy
6
8
10
12
14
nucleon number A
exp.
(a)
(b)

Fig.2

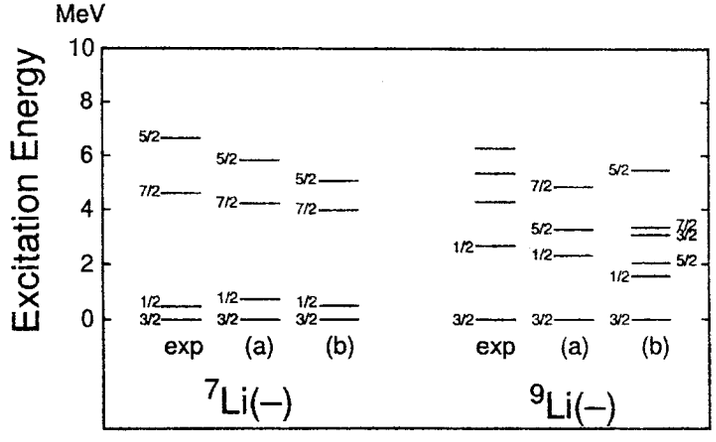
MeV
Excitation Energy
10
8
6
4
2
0
5/2
7/2
1/2
3/2
exp
(a)
(b)
^{7}Li(–)
^{9}Li(–)

Fig.3

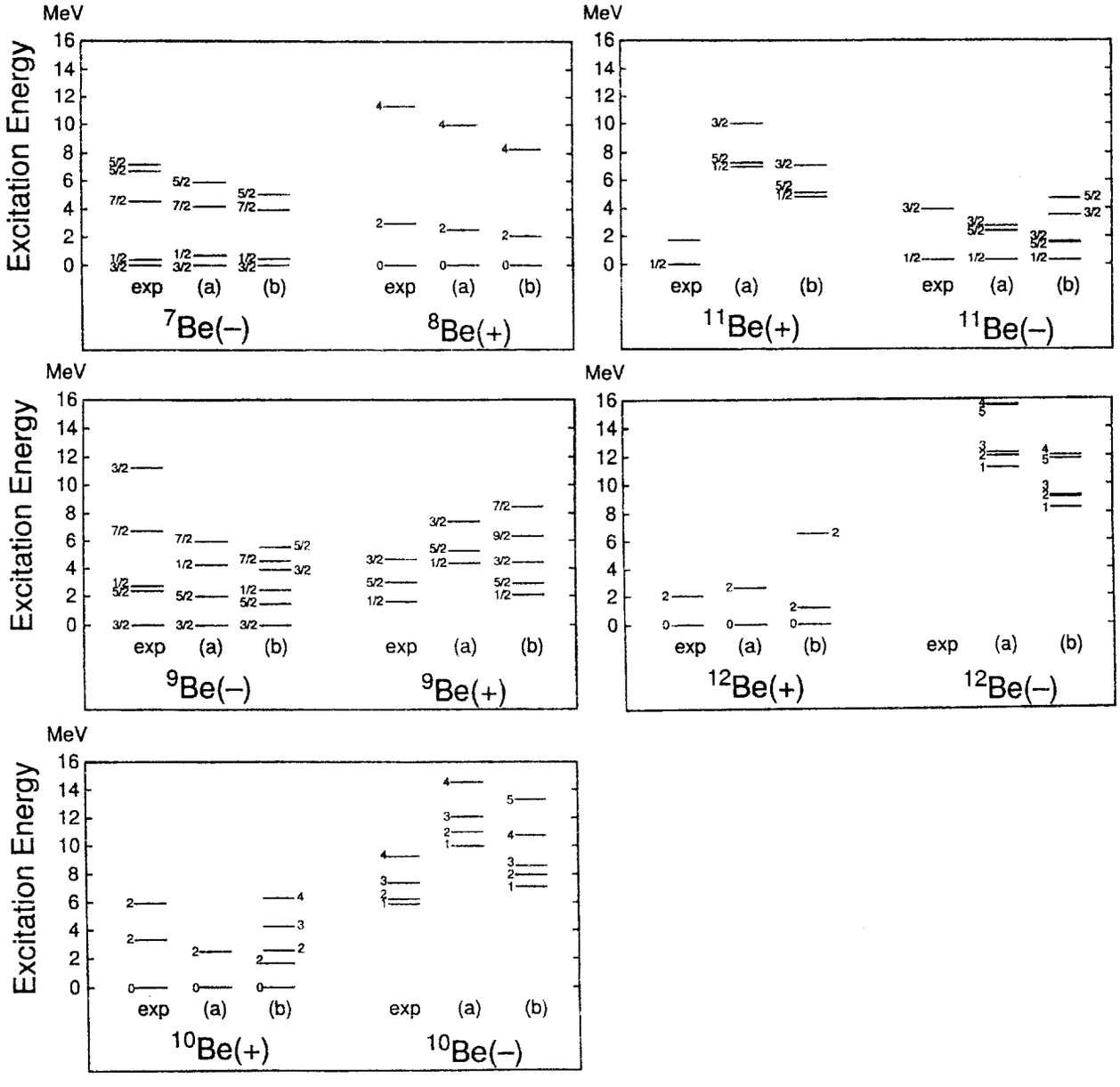
MeV
Excitation Energy
exp (a) (b)
^{7}Be(−)
^{8}Be(+)
^{11}Be(+)
^{11}Be(−)
^{9}Be(−)
^{9}Be(+)
^{12}Be(+)
^{12}Be(−)
^{10}Be(+)
^{10}Be(−)

Fig.4

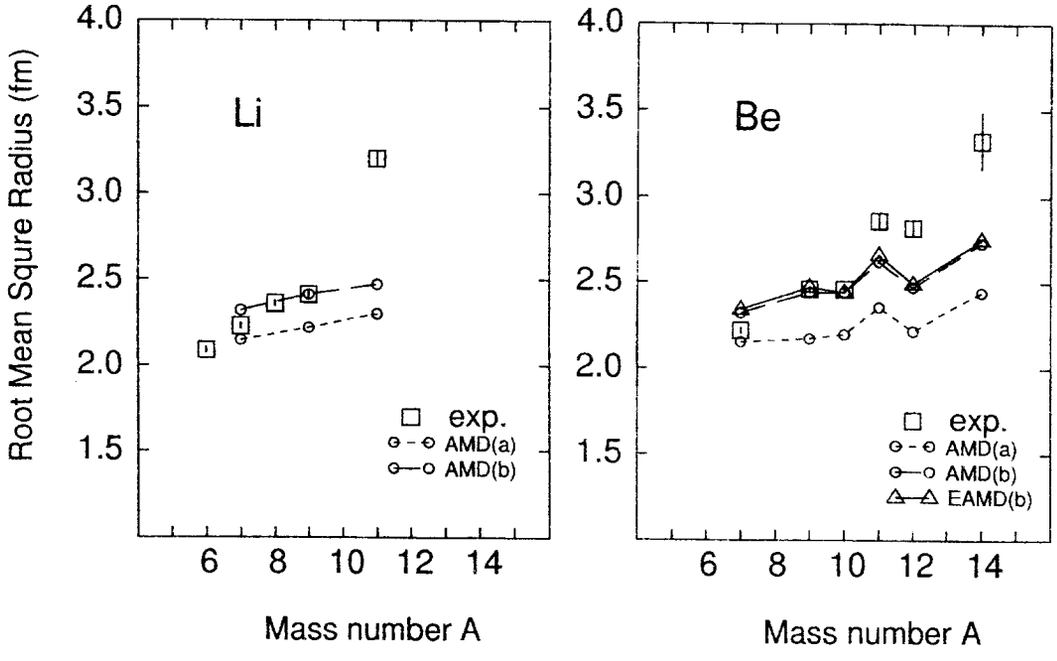
Root Mean Squre Radius (fm)
4.0
3.5
3.0
2.5
2.0
1.5
Li
exp.
AMD(a)
AMD(b)
6
8
10
12
14
Mass number A
Be
exp.
AMD(a)
AMD(b)
EAMD(b)
Mass number A

Fig.5

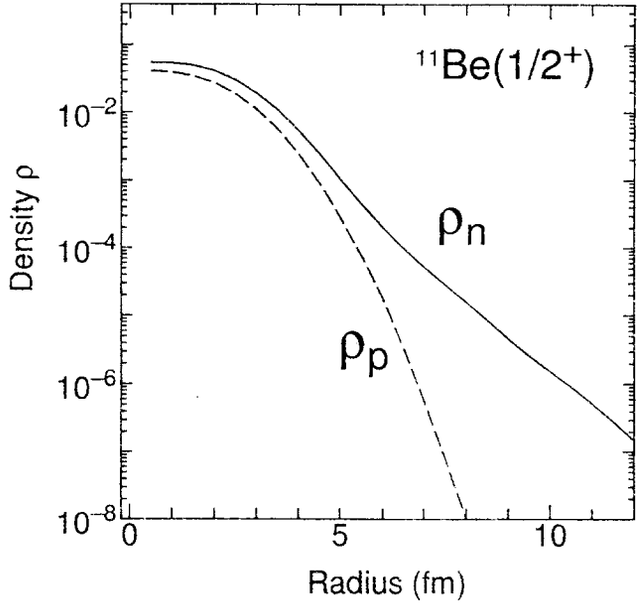
^{11}Be(1/2$^+$)
Density ρ
10^{-2}
10^{-4}
10^{-6}
10^{-8}
ρ_n
ρ_p
0
5
10
Radius (fm)

Fig.6

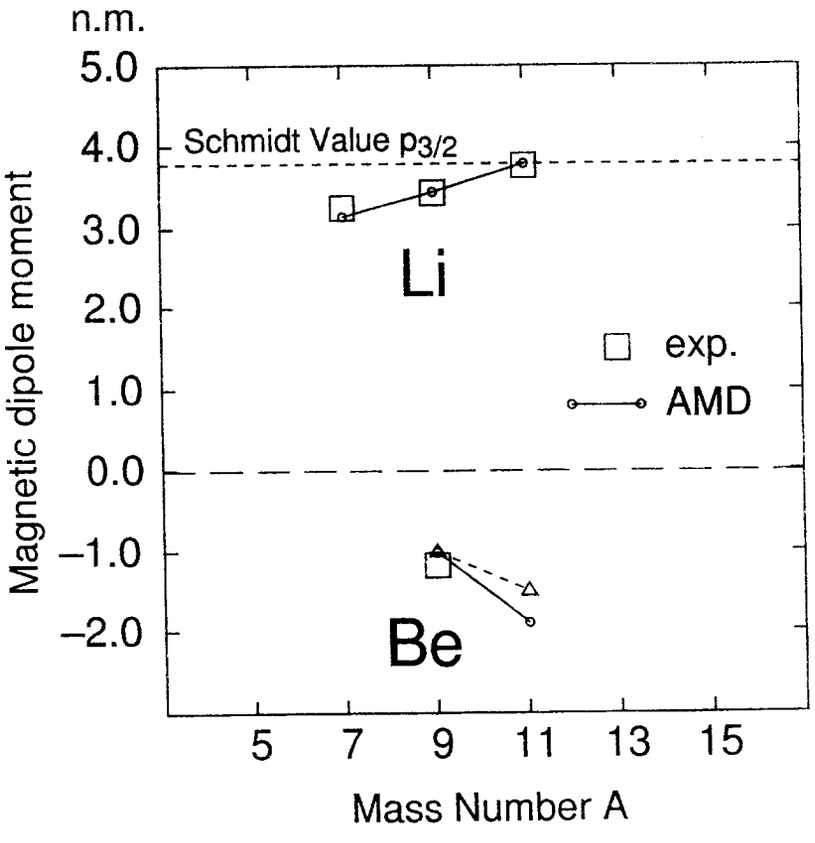
n.m.
5.0
4.0
3.0
2.0
1.0
0.0
−1.0
−2.0
Schmidt Value $p_{3/2}$
Li
Be
exp.
AMD
Magnetic dipole moment
5
7
9
11
13
15
Mass Number A

Fig.7

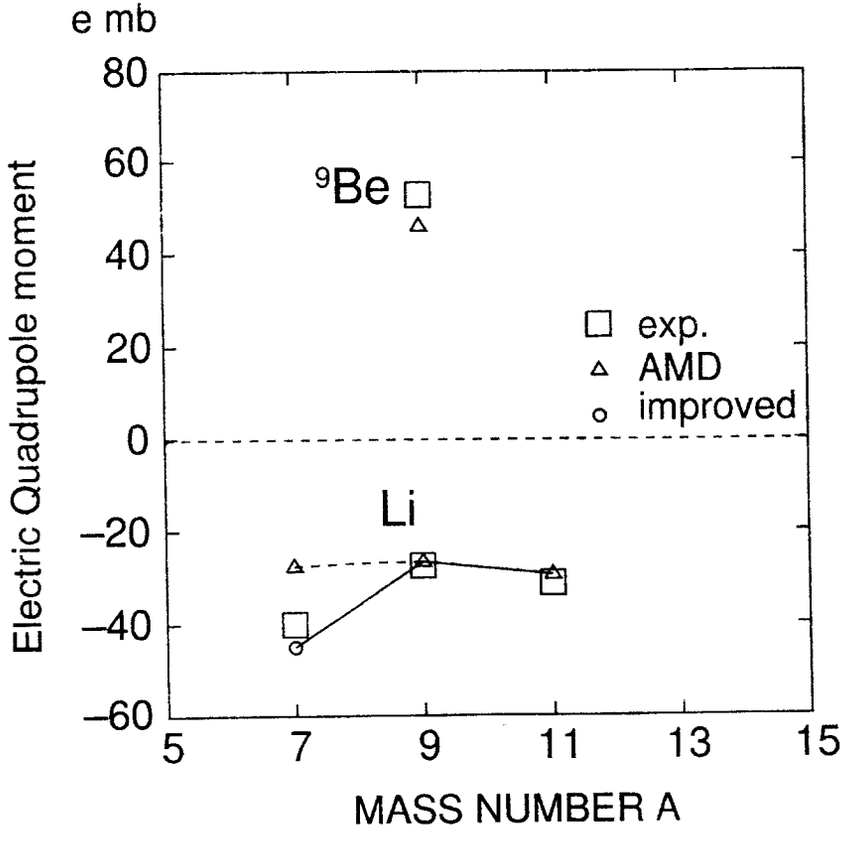
e mb
80
60
40
20
0
−20
−40
−60
^{9}Be
Li
exp.
AMD
improved
Electric Quadrupole moment
5
7
9
11
13
15
MASS NUMBER A

Fig.8

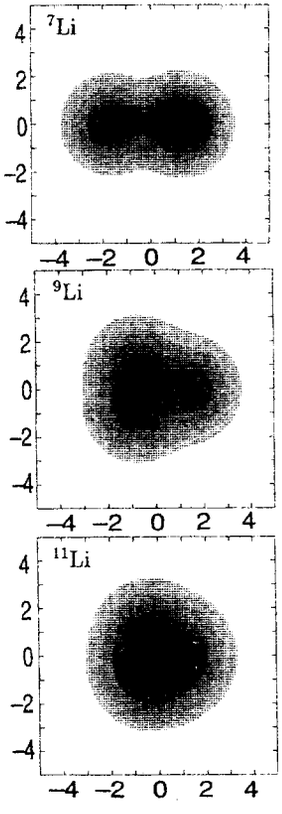

Fig.9

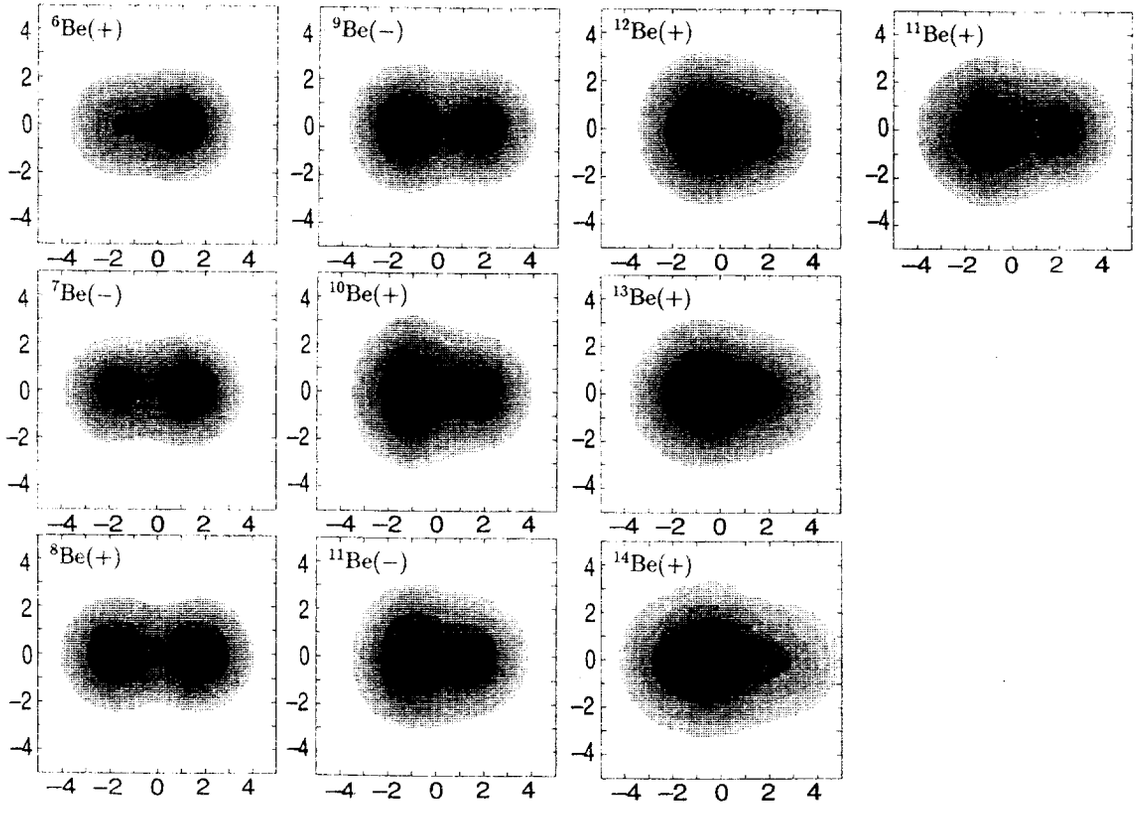

Fig.10

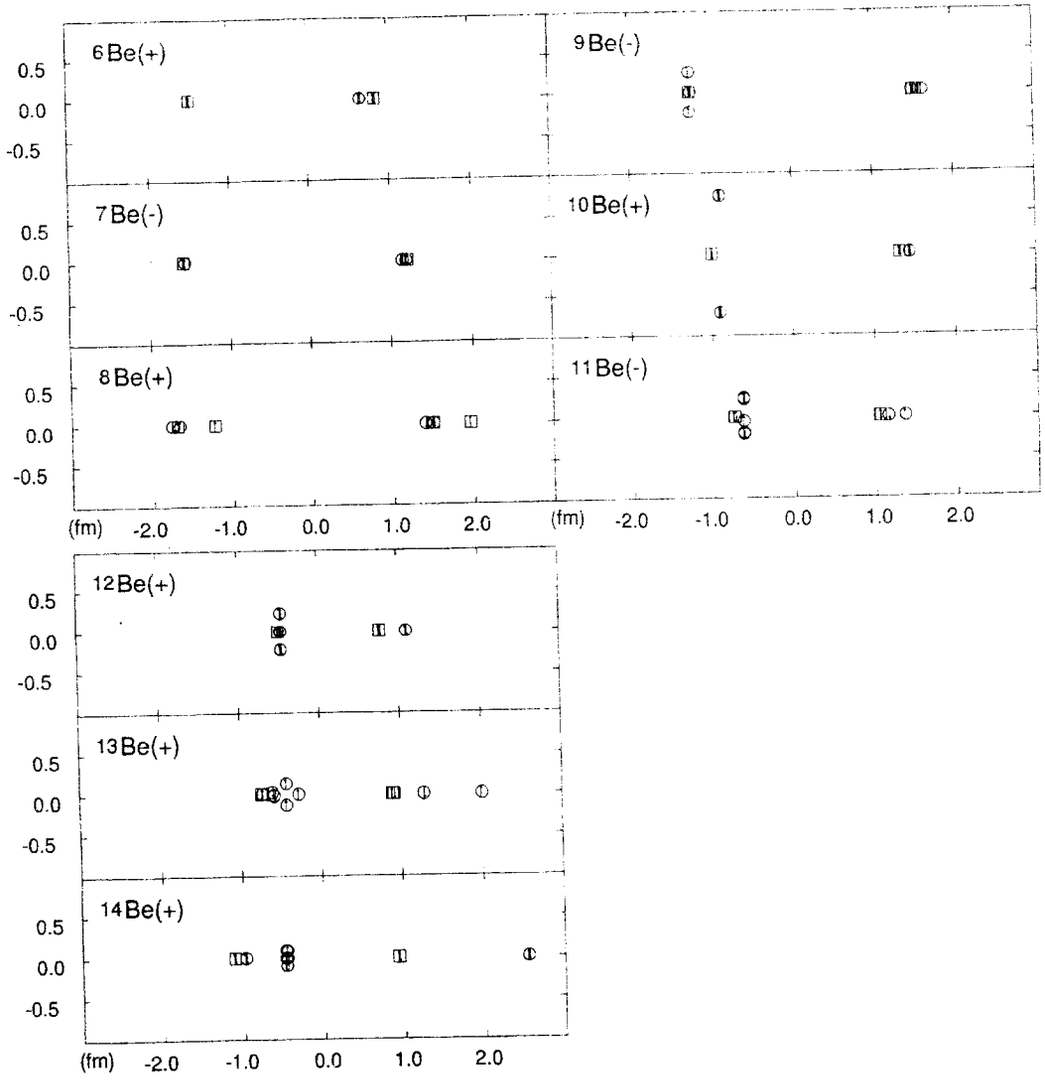
6Be(+)
9Be(-)
7Be(-)
10Be(+)
8Be(+)
11Be(-)
12Be(+)
13Be(+)
14Be(+)
0.5
0.0
-0.5
(fm)
-2.0
-1.0
0.0
1.0
2.0

Fig.11

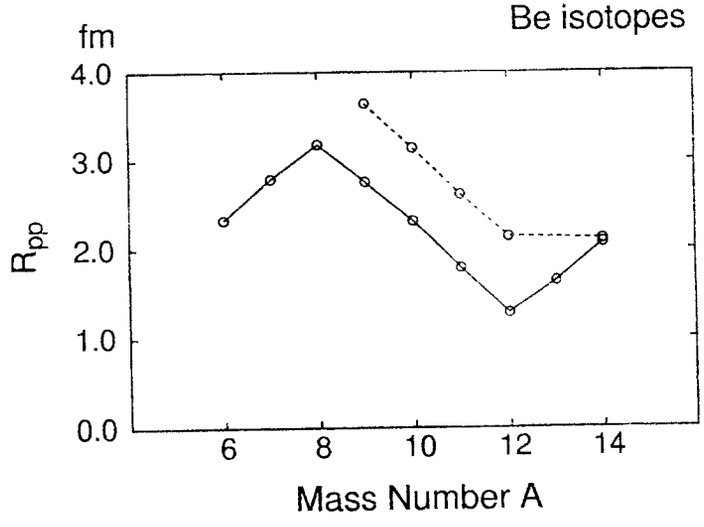
Be isotopes
fm
R_{pp}
4.0
3.0
2.0
1.0
0.0
6
8
10
12
14
Mass Number A

Fig.12

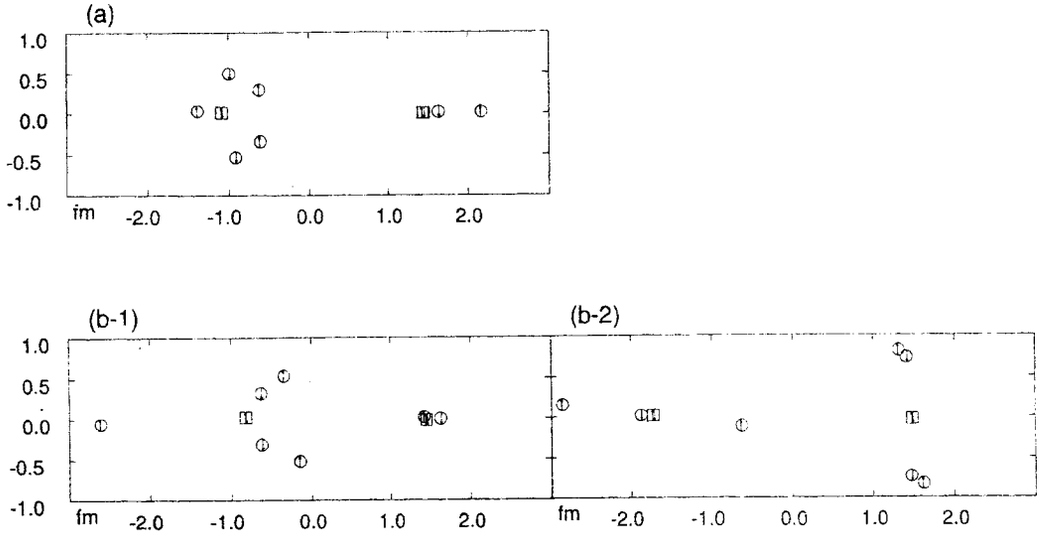
(a)
1.0
0.5
0.0
-0.5
-1.0
fm
-2.0
-1.0
0.0
1.0
2.0
(b-1)
(b-2)

Fig.13

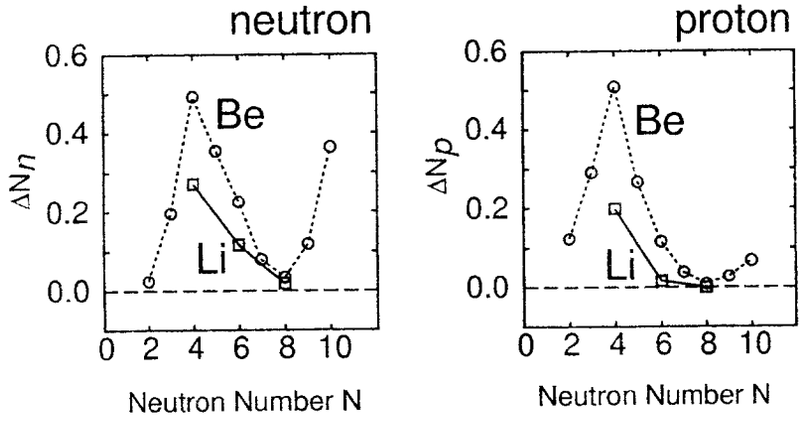
neutron
proton
Be
Li
ΔN_n
ΔN_p
0.6
0.4
0.2
0.0
0 2 4 6 8 10
Neutron Number N